The Meteoritical Society

Meteoritics & Planetary Science 44, Nr 10, 1489–1509 (2009)
Abstract available online at http://meteoritics.org

Interpretation of Wild 2 dust fine structure: Comparison of Stardust aluminum foil craters to the three-dimensional shape of experimental impacts by artificial aggregate particles and meteorite powders

A. T. KEARSLEY[1*], M. J. BURCHELL[2], M. C. PRICE[2], G. A. GRAHAM[1], P. J. WOZNIAKIEWICZ[1, 3], M. J. COLE[2], N. J. FOSTER[2], and N. TESLICH[3]

[1]IARC, Department of Mineralogy, The Natural History Museum, London SW7 5BD, UK
[2]Centre for Astrophysics and Planetary Sciences, School of Physical Science, University of Kent, Canterbury CT2 7NH, UK
[3]Institute of Geophysics and Planetary Physics, Lawrence Livermore National Laboratory, 7000 East Avenue, Livermore, California 94550, USA
[*]Corresponding author. E-mail: antk@nhm.ac.uk

(Received 11 March 2009; revision accepted 14 September 2009)

Abstract–New experimental results show that Stardust crater morphology is consistent with interpretation of many larger Wild 2 dust grains being aggregates, albeit most of low porosity and therefore relatively high density. The majority of large Stardust grains (i.e. those carrying most of the cometary dust mass) probably had density of 2.4 g cm^{-3} (similar to soda-lime glass used in earlier calibration experiments) or greater, and porosity of 25% or less, akin to consolidated carbonaceous chondrite meteorites, and much lower than the 80% suggested for fractal dust aggregates. Although better size calibration is required for interpretation of the very smallest impacting grains, we suggest that aggregates could have dense components dominated by μm-scale and smaller sub-grains. If porosity of the Wild 2 nucleus is high, with similar bulk density to other comets, much of the pore space may be at a scale of tens of micrometers, between coarser, denser grains.

Successful demonstration of aggregate projectile impacts in the laboratory now opens the possibility of experiments to further constrain the conditions for creation of bulbous (Type C) tracks in aerogel, which we have observed in recent shots. We are also using mixed mineral aggregates to document differential survival of pristine composition and crystalline structure in diverse fine-grained components of aggregate cometary dust analogues, impacted onto both foil and aerogel under Stardust encounter conditions.

INTRODUCTION

The materials returned from comet Wild 2 by the Stardust mission (Brownlee et al. 2003, 2006) have already offered an opportunity to interpret the composition (Flynn et al. 2006), mineralogy (Zolensky et al. 2006) and grain size distribution (Hörz et al. 2006) for samples from a Jupiter family comet. To understand the fine internal structure of the dust is also important for several reasons. It may reveal the scale of juxtaposition of unequilibrated materials, the mechanism of their aggregation, and the extent of subsequent compaction, textural and compositional equilibration. Together, these may help to explain the internal structure of the cometary nucleus, and allow us to test the models proposed for its accretion (e.g., Donn 1990, 1991) and evolution (e.g., Belten et al. 2007). Inevitably, study of truly pristine cometary dust structure is compromised by the mechanisms of dust release that result in grain disaggregation (Clark et al. 2004) and loss of volatile molecular species within the coma (e.g., Cottin et al. 2004; Dello Russo et al. 2006). These processes undoubtedly modify the dust, yet also produce the materials whose properties can be studied by remote sensing. The Stardust samples should therefore provide valuable "ground-truth" data for comparison to spectroscopic and laboratory observations (e.g., Levasseur-Regourd et al. 2008). However, hypervelocity particle capture may complicate interpretation of the collected dust (see review by Burchell and Kearsley 2009). Although silica aerogel (Hörz et al. 1998) is probably the best medium currently available for the capture of grains at high speeds, numerous authors have now demonstrated that the complexity of particle disaggregation (Zolensky et al. 2008), surface abrasion and melting (Hörz et al. 2009; Burchell et al.

2006, 2009), decomposition (Noguchi et al. 2007; Velbel and Harvey 2007) and mixing with aerogel (Leroux et al. 2008a) can make original grain size and internal structure difficult to determine. For relatively robust, coarse (>10 μm), dense (>2 g cm^{-3}) impactors, the development of characteristic "carrot-shaped" aerogel tracks (Type A of Burchell et al. 2008) is now well documented, and a particle size calibration is possible (Burchell et al. 2008). The origin of more complex aerogel track shapes has been addressed in a theoretical treatment by Trigo-Rodríguez et al. (2008), who conclude that shock-driven break-up of weakly-bonded aggregate particles, and disintegration also partially driven by volatile expansion, is responsible for "bulbous" tracks (Type C of Burchell et al. 2008). Where an aggregate impactor also contains a larger, well consolidated grain, an intermediate Type B track is observed with a bulb followed by a carrot like track emerging from it. The Stardust aluminum foils show impacts by a wide size range of grains (Hörz et al. 2006), of which some had a complex porous aggregate structure with diverse internal composition (Kearsley et al. 2008a). In this paper we describe experiments using projectiles with complex internal structure and constrained sub-grain dimensions, and their implications for the interpretation of Wild 2 grains.

Cometary Dust Structure

Size and structure of cometary dust have been investigated by both remote sensing (e.g., Hanner 1984) and by microscopy of samples attributed to a cometary origin but collected in the stratosphere (e.g., Rietmeijer and MacKinnon 1987), as well as by theoretical modeling of dust and ice accretion in the environments of interstellar (IS) space and dense molecular clouds (DMC), e.g., Greenberg et al. (1989), Iatì et al. (2004). Dust size and mass were measured by optical and impact sensor instruments during the comet Halley encounter (Fulle et al. 2000), showing a substantial proportion of coarser (>>micrometer) grains. Nevertheless, before the first samples were returned by the Stardust mission from comet Wild 2 in 2006, a popular conception of cometary dust envisaged an abundance of fine micrometer-scale particles of IS origin, made of loosely connected nanometer-scale aggregates of poorly crystalline or amorphous silicate and carbonaceous material, mantled by ices, and forming a low-density, very porous "fluff" (Greenberg 1987). An alternative view emphasized the similarity of Halley dust to anhydrous interplanetary dust particles (IDPs) collected in the stratosphere (Brownlee et al. 1987), noting the more complex internal heterogeneity of IDPs, compared to the Greenberg model. Porous structure has certainly been observed frequently in IDPs, in some of which the presence of abundant "glass with embedded metal and sulfides" (GEMS; Bradley 2004) and grains with exotic "presolar" isotopic signatures (e.g., Nguyen et al. 2007) indicate little equilibration and the survival of primitive composition and structure in IS dust gathered into a cometary nucleus. However, Zhukovska et al. (2008), conclude that the majority of crystalline grains should lose their distinctive structural, chemical and isotopic signatures to amorphization and homogenization within aggressive IS and DMC environments, leaving few survivors. Greenberg et al. (1989) had suggested that processing within DMC might yield concentrically layered deposits upon amorphous silicate grain nuclei, which then aggregate into a very low density and high porosity framework. Experiments with fine particles under realistic early nebular conditions of dust size and density, gas pressure and flow rate have also produced complex branching aggregates (Blum and Wurm 2000; Dominik et al. 2007) indicating that they could form in the earliest stages of planetesimal accretion, and do not have to be inherited from presolar environments. Indeed, fractal aggregate particles with porous, branching structure have been invoked to account for discrepancies between different spectroscopic measurements of grain size in nebular and circumstellar dust (Nakamura, 1998). The low bulk density measurements made for many comet nuclei (see discussions by Weissmann et al. 2005; Levasseur-Regourd et al. 2009) including Wild 2 (Davidsson and Gutiérrez 2006) certainly suggest there must be substantial internal porosity, but at what physical scale? Is the pore space within fine fractal aggregates, or between coarser, denser grains?

It is now apparent that not all comets are dominated by fine, low density porous dust made of sub-micrometer grain aggregates. Telescopic observations of cometary comae (e.g., Jewitt and Meech 1986; Jewitt and Matthews 1999) have shown that coarser material may be abundant. Interpretation of meteor observations by Trigo-Rodríguez and Llorca (2006) also suggest variation in strength properties for cometary micrometeoroids from different sources, possibly as a function of compaction (implying differences in grain density). Spacecraft encounters such as Stardust (Tuzzolino et al. 2004) have confirmed that micrometer and coarser materials may be present in substantial quantity, and that much may be crystalline (Brownlee et al. 2006; Zolensky et al. 2006, 2008). The internal structure of some of the more robust aggregate Wild 2 cometary grains has been revealed by transmission electron microscopy (TEM) of ultra-thin sections cut from Stardust aerogel terminal particles (Brownlee et al. 2006), and innovative synchrotron X-ray computed microtomography has shown textural relationships between minerals reminiscent of chondrules (Nakamura et al. 2008). Unfortunately, it is clear from synchrotron X-ray fluorescence maps of elemental composition that disruption and segregation of particle components occurs in the majority of aerogel tracks (Flynn et al. 2006; Flynn 2008; Lanzirotti et al. 2008). Careful analysis of both coarser and finer materials on the walls of bulbous aerogel tracks by time-of-flight secondary ion mass spectrometry (TOF-SIMS) suggests that

many of the dispersed sub-micrometer components may have had a composition close to CI chondrite meteorites (Stephan et al. 2008). We do not yet know whether this type of fine material was present as a jacket around most of the more robust terminal grains prior to their collection, making the particles effectively aggregates, of which only the coarser sub-grains are now easy to see. To better understand the original properties of the cometary dust collected by the Stardust mission it is therefore helpful to be able to simulate the modification of their structure and composition during their hypervelocity impact onto the collection media. Not only does this allow us to interpret the overall density and porosity of the grains (Kearsley et al. 2008b), but also to assess how compositional heterogeneity in the impact residue may reflect fine structure within the particle. Although the recognition of real, pristine amorphous material in aerogel tracks is fraught with difficulties (Ishii et al. 2008), results from small craters on the aluminum foils (Leroux et al. 2008b) suggest that these may also be a good place to evaluate the contributions of crystalline and amorphous materials to Wild 2 dust.

Aluminum Foil Craters

The flight of Stardust through the coma of comet 81P/Wild 2 (Tsou et al. 2004) yielded a harvest of dust, captured in low density silica aerogel, and impacted onto surrounding aluminum (Al) foil sheets (Brownlee et al. 2006; Hörz et al. 2006). The relatively low peak pressure (estimated at <1 GPa, e.g., Trigo-Rodríguez et al. 2008) experienced by particles ploughing into aerogel at 6.1 km s^{-1} allowed survival of diverse original grain compositions (Zolensky et al. 2006) and crystalline structure (Ohsumi et al. 2008). However, as suggested might occur by Graham et al. (2001), abrasion and sub-grain disaggregation disrupted fragile components, making it difficult to interpret the original particle structure. The complexity of particle interaction with aerogel is now being revealed in laboratory experiments (Ishii et al. 2008; Leroux et al. 2008a) and numerical impact simulations (Dominguez et al. 2004).

Impact of grains upon the spacecraft aluminum foils inevitably created higher shock pressures (estimated in the range 60–80 GPa, e.g., Burchell and Kearsley 2009), and hence more extreme structural and sometimes compositional processing of the impactor (Wozniakiewicz et al. 2008). There are also a suite of confusing artifacts associated with the composition and fabrication of the foil sheets (see discussion below). Nevertheless, analysis of residues on the foils (Kearsley et al. 2008a; Leitner et al. 2008) has yielded useful compositional information, and interpretation of the size and shape of the impacting particles may be more straightforward from foil craters than from aerogel tracks. There is a long history of experimental studies on the response of metal targets to hypervelocity impact (e.g., Cour-Palais 1987; Bernhard and Hörz 1995; Kearsley et al. 2006), and the relationship between the characteristics of impactors and crater shape is currently probably better understood than the processes responsible for aerogel track morphology, for which systematic experimentation (e.g., Burchell et al. 2008, 2009) and modeling (e.g., Trigo-Rodríguez et al. 2008) are still in progress. Using sophisticated image acquisition and analysis methods, we can now describe the three dimensional shape of Stardust foil craters, and interpret the properties of dust grains responsible by comparison to impact features created under analogous laboratory conditions (Kearsley et al. 2007) using light gas gun (LGG) shots. Our earlier work employed powder projectiles from a wide range of glass, metal and mineral powders (Kearsley et al. 2008b) to document the influence of impactor species upon crater morphology and size, and to make comparison to Stardust craters with simple shape (e.g., Fig. 1). Recent development of complex artificial projectiles which can be fine-grained, porous, and of relatively low density (Kearsley et al. 2008a, 2008b) has also allowed more realistic simulation of impact by aggregate particles. In this paper we document impacts by artificial aggregates, compare them to Stardust craters with both simple bowl shapes and more complicated internal morphology, and explain how they help us to understand the internal structure, especially density and porosity, of Wild 2 dust.

MATERIALS AND METHODS OF STUDY

Stardust foils from the cometary side of the collector were examined by scanning electron microscopy (SEM) as part of the preliminary examination (PE), Hörz et al. (2006) and Kearsley et al. (2008a). Additional stereo imagery of smaller craters was based on subsequent sample allocations, especially foil C011N,1 (which is from a location between aerogel tiles with numerous small tracks, and bears a large number of small craters), foil C092W,1 and foil C050W,1. Flight spare 101 μm thickness Al 1100 foils were supplied by NASA for use as targets in our LGG experimental shots at the University of Kent, using the technique of Burchell et al. (1999). All targets were left unprepared, with no application of a conductive coating, and will be archived at the Natural History Museum (NHM), London for further research. Imagery was performed on a JEOL 5900LV SEM, in both backscattered electron (BEI) and secondary electron (SEI) modes. Stereo pair images were collected with 6 degree angular separation (the foil being tilted to 3 degrees either side of perpendicular). False color anaglyph images were created by overlaying red positive tilt (left aspect) images upon cyan negative tilt (right aspect) images, with careful spatial registration. Gross crater morphology is then readily apparent, and allows recognition of “simple bowl” and complicated “compound” crater morphology (Kearsley et al. 2008a). Alicona MeX 4.2 software was used to generate

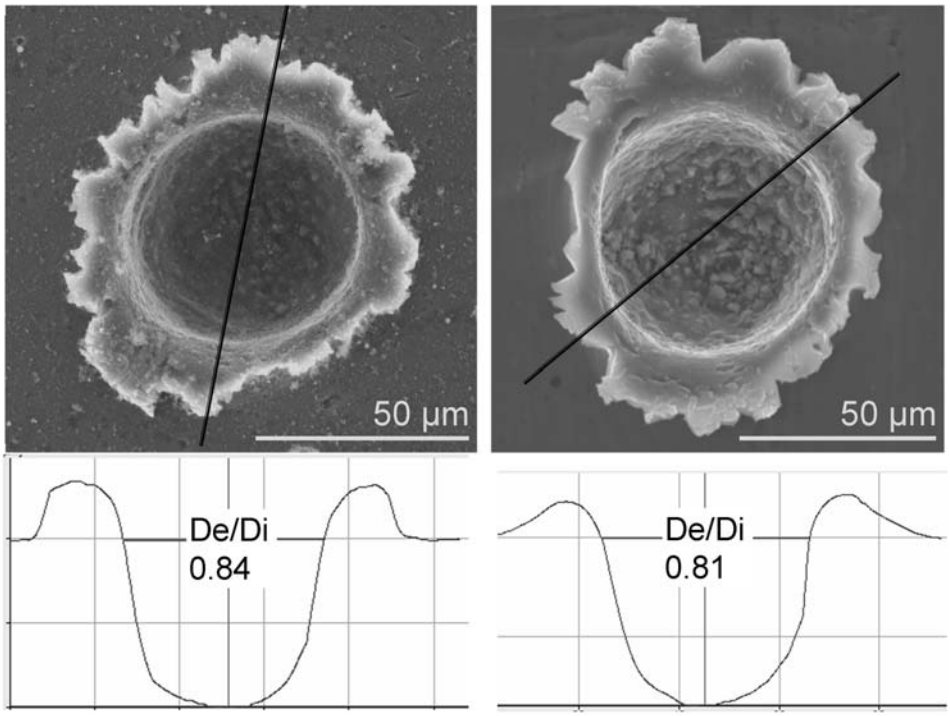

Fig. 1. Secondary electron images (SEI) of large bowl-shaped craters on Al 1100 foil, impact velocity ~6.1 km s^{-1}, created by: (left) an experimental olivine grain, Forsterite (Fo) 88%; and (right) Wild 2 dust, crystalline Fo 97% olivine (Kearsley et al. 2008b). MeX digital elevation model depth profiles from the lines indicated on the images, show similar "simple bowl" morphology. Note abundant angular impactor debris on the floor of both craters, and that the depth to diameter (De/Di) ratio is almost at the top of the range seen in experimental olivine impacts.

digital elevation models (DEM) from the stereo-pairs, using the protocols of Kearsley et al. (2008a and b). Color-coded three-dimensional depth models from MeX reveal the detailed crater form in contours, and following definition of the pre-impact ambient plane in the DEM, crater diameter (Di) and depth (De) were measured from representative cross-sections (e.g., Fig. 1). The De/Di values were compared to experimental data for mineral projectiles of known density, from Kearsley et al. (2008b) and new data presented below. To exclude impact features created by gun debris, and to positively identify impacts by complex polymineralic aggregates, X-ray mapping and spectrum acquisition were performed using the SmartMap routines of the Oxford Instruments INCA system fitted to the SEM.

Experimental Projectiles

Six types of dust analogue aggregates were produced from mineral powders selected and prepared from the mineral projectile collection of the NHM, using variants of the adhesive spray droplet impregnation method described by Kearsley et al. (2008b). Samples of the aggregates were examined by SEM to characterize textural and compositional internal heterogeneity and particularly to assess relative volumetric proportions of their components, and bulk aggregate porosity and density. Average density and porosity values for the two sets of polymineralic aggregates and the monomineralic monodisperse olivine aggregates were calculated from measured areas of impregnating resin, adhesive and mineral matter in SEM images of polished sections. Values for the monomineralic enstatite and lizardite aggregates are estimates based upon surface imagery of stub-mounted aggregate particles. For the lizardite aggregates, the unfilled porosity figure also includes ~15% sub-micrometer intra-granular porosity, as revealed in high magnification imagery of polished sections of the mineral sample before powder preparation. Values of bulk density and porosity for grains in our powders of Allende (CV3) and Orgueil (CI) are taken from Consolmagno et al. (2008), although we also note that Corrigan et al. (1997) suggest a much lower porosity value (4%) should be used for unaltered Orgueil matrix. In finer grained portions of aggregates made from polydisperse powders, relative proportions of adhesive and unfilled porosity are extremely difficult to measure accurately (Table 1), and fluctuate due to the heterogeneous grain size and shape distribution. Although not a critical issue for the first experiments (demonstrating technical feasibility of simulating aggregate impacts), this became an important limitation in interpretation of particle properties when considering detailed mechanisms for crater excavation.

The first artificial aggregates were produced from a mixture of olivine, diopside and pyrrhotite, separately powdered in a pestle and mortar, producing polydisperse

Table 1. Aggregates and meteorite powders used as projectiles in this study.

Shots	Velocity (km s^{-1})	Mineral components	Component size range	Adhesive	Estimated density ρ and porosity volume %
G200207#1 G200207#2 G200207#3	4.63 5.07 4.68	Polymineralic: Olivine, Diopside, Pyrrhotite	Polydisperse 1–200 μm	Acrylate 1 PVA Acrylate 2	ρ Low ~1.9 g cm^{-3} porosity very variable unfilled pores avg. 24% filled porosity avg. 35%
G290607#1	5.98	Monomineralic Enstatite	Polydisperse 1–200 μm	Acrylate 1	ρ Low ~1.9 g cm^{-3} porosity very variable unfilled pores ~25% filled porosity ~25%
G290607#2	6.03	Monomineralic Lizardite	Polydisperse 1–200 μm	Acrylate 1	ρ Low ~1.2 g cm^{-3} unfilled pores ~40% filled porosity ~25%
G210208#2 G091008#1	6.30 6.00	Monomineralic Olivine	Monodisperse 0.3–8 μm, 3 μm mode	Acrylate 1 Acrylate 1	ρ High, avg. ~2.4 g cm^{-3} filled porosity 30–66%
G221208#1	6.03	Polydisperse Olivine, Diopside, Pyrrhotite	Monodisperse Silicates 0.3–8 μm; Sulfide 90% <10 μm	Acrylate 1	ρ High, avg. ~2.4 g cm^{-3} porosity very variable unfilled pores ~0% filled porosity 30–66%
G301106#1	5.95	Allende CV3: (diverse silicates, Fe sulfides)	Polymineralic <125 μm	None	ρ 2.79 g cm^{-3} unfilled pores ~23%
G220405#3	6.19	Orgueil CI1: (phyllosilicates, Fe oxides, Fe sulfides, Ca phosphates)	Polydisperse Most 38–54 μm	None	ρ 1.6 g cm^{-3} unfilled pores 4–35?%

powders, and then mixed together without deliberate size separation. Three types of adhesives were tested: acrylate spray sold as Windsor and Newton fixative (Acrylate 1); a second commercial acrylate aerosol (Acrylate 2); and an aqueous solution of poly vinylacetate (PVA). Each was sprayed as fine droplets onto the gently agitated surface of loose powder, to encourage loose grain-to-grain adhesion, creating aggregates with high porosity and low overall density (Fig. 2). Cross sections through these aggregates (Kearsley et al. 2008b) revealed a thin adhesive coating on loosely held coarser grains touching at a few points and giving high porosity at scales of tens of micrometers, but a relatively weak structure. In finer-grained portions of the aggregate, adhesive infills all of the pore space between grains yielding a denser and stronger structure. All three adhesives successfully bound the polymineralic powder mixture into aggregates, although the ease of application for the acrylate aerosol spray proved the most convenient. In the initial shots to test the survival of aggregates in LGG shots, the projectiles were fired at polished Al 6000 series targets, thereby conserving valuable Stardust foil during the proving shots. The impact velocity was between 4.6 and 5.1 km s^{-1}, lower than the Stardust Wild 2 encounter velocity (6.1 km s^{-1}). Following the first shot, which was successful, further aggregates were produced from polydisperse enstatite and lizardite powders. However, as all of these low density polydisperse aggregates yielded relatively few distinctive impacts (see results section below), a second method of aggregate production was attempted.

The finest grain-size olivine aggregates were produced from carefully picked grains of San Carlos olivine, powdered

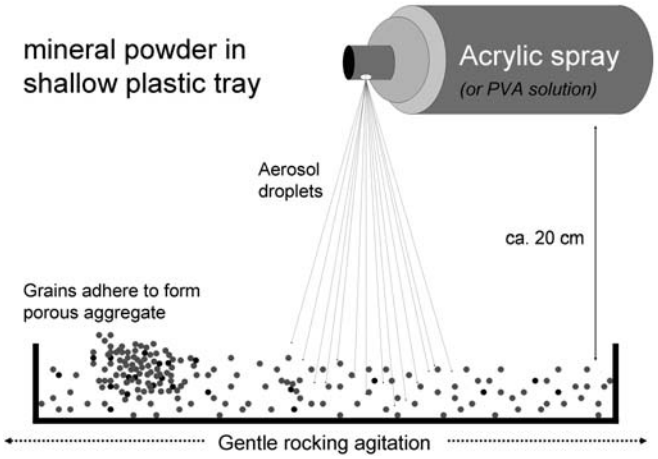

Fig. 2. Schematic of process for creation of polydisperse low-density aggregate projectiles.

in a vibratory disc mill (made by TEMA Machinery Ltd.). The powder was made into an aqueous slurry, and a column cylinder was used to sediment all grains coarser than 8 μm, by timed deposition. The cloudy supernatant fluid was pipetted into a second sedimentation column, and fines were concentrated by long sedimentation (1 week). Removal of supernatant fluid, and drying of the concentrated slurry yielded a fine powder with grain size range from <8 μm down to sub-μm, and a mode ~3 μm. The fine grain size made powder agitation for aggregate production very difficult, as much was lost by suspension into the cabinet airflow (necessary for safe handling of materials <10 μm in size). To

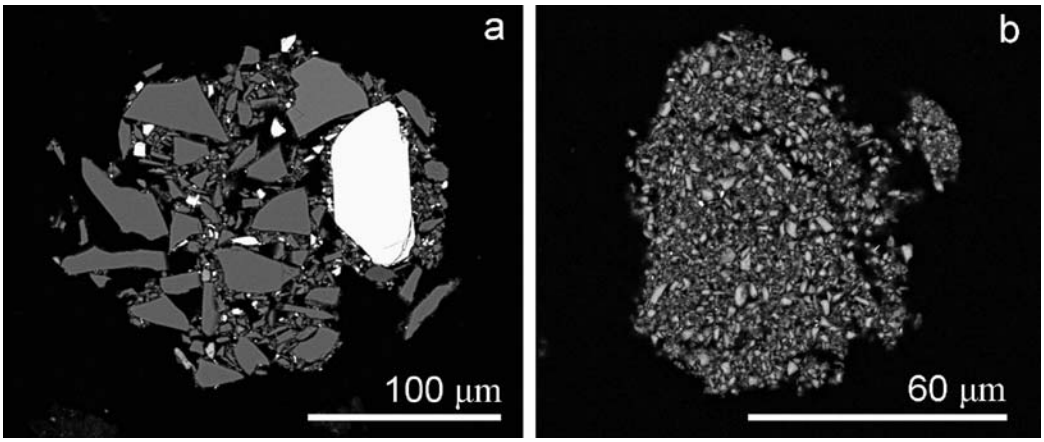

Fig. 3. a) BEI of a cross section through a polymineralic, polydisperse, low density, high porosity aggregate projectile. Dark areas are pore space filled by resin (both adhesive and block impregnating resin for sectioning), mid grey areas are silicate minerals, bright areas are sulfide. b) BEI of a cross section through a monodisperse, monomineralic, high-density, low-porosity aggregate projectile made of fine olivine. Mid grey areas are olivine, dark areas are porosity filled by acrylate resin.

improve the yield of aggregates, a small quantity of the powder was therefore placed in a watch-glass, made into a fine dilute slurry with distilled water, and placed on a hot plate, where it was allowed to dry into a thin powder cake. The surface of the cake was then sprayed with acrylate adhesive until a glossy surface was seen (implying filling of all available pore-space), and again allowed to dry on the hot plate. The solid mixture was gently scraped free of the underlying glass surface, yielding rolled slivers of material. In the dry cake, assuming sub spherical grain shape and high efficiency grain packing, the powder could be expected to have a porosity between 26 and 48%, available for infill by acrylate resin during aggregate production. Grain angularity and relatively broad grain size range (sub μm to ~3 μm dominant) can result in deviation from a simple close-pack model. Area analyses of ten BEI taken at high magnification on polished sections through the olivine aggregates (e.g., Fig. 3b) revealed that the proportion of resin to olivine varied from 30:70 to 66:34, with an average of 49:51. Were all of the space between olivine grains (3.2 g cm^{-3}) completely filled by acrylate (1.175 g cm^{-3}) this would yield an average density of 2.2 g cm^{-3} for these aggregates. However, portions of aggregates with substantial unfilled pore space (and apparently low olivine proportion) are likely to be relatively weak, causing fragmentation during acceleration in the LGG. The density of impacting coarser aggregates was thus likely to be biased towards the higher end of the range, nearer 2.4 g cm^{-3}.

A similar preparation protocol was used to produce a fine diopside powder. Although TEMA preparation of sulfides was also straightforward, size separation of pyrrhotite proved more difficult due to magnetic attraction of fine grains causing rapid clumping and sedimentation from suspension. A small quantity of <10 μm pyrrhotite was successfully separated by drawing dry powder through a fine filter, using a strong magnet. However, during later stages of aggregate production, the fine pyrrhotite was again prone to clumping, and to prevent excessive segregation encouraged by powder agitation, the polymineralic components were gently mixed as a dense slurry in a droplet of distilled water and allowed to dry as a paste in an evaporating dish. The surface of the dry powder cake was then impregnated by acrylic spray until all porosity was assumed to be filled. SEM imagery shows that the resulting aggregates do contain more adhesive and less pore space than in our earlier experiments (Kearsley et al. 2008b), and in-flight fragmentation releasing smaller particles dominated by adhesive might therefore be expected to yield some proportion of impacts by organic rather than mineral components.

Crushed samples of two carbonaceous chondrite meteorites had also been prepared as projectiles for earlier work in 2005 and 2006. The complex, heterogeneous mineral distribution within meteorite samples leads to uncertainty as to the precise composition of the particle responsible for an individual impact feature. and our previous studies of cratering had therefore been largely confined to projectiles of well-characterized composition. In the light of our new results from artificial aggregate impacts, we have re-examined the target foils and plates impacted by meteorite powders, not only to determine the distribution of residue from particular meteorite mineral components, but particularly to document the detailed three dimensional crater shapes.

The higher density, lower porosity monodisperse aggregates and meteorite powders were all fired at velocities close to 6 km s^{-1}, onto targets of flight-spare Stardust foil.

RESULTS FROM STARDUST

The preliminary examination of Stardust foils revealed that four (probably five) of the seven large (>20 μm diameter) Stardust impact features examined (Kearsley et al. 2008a)

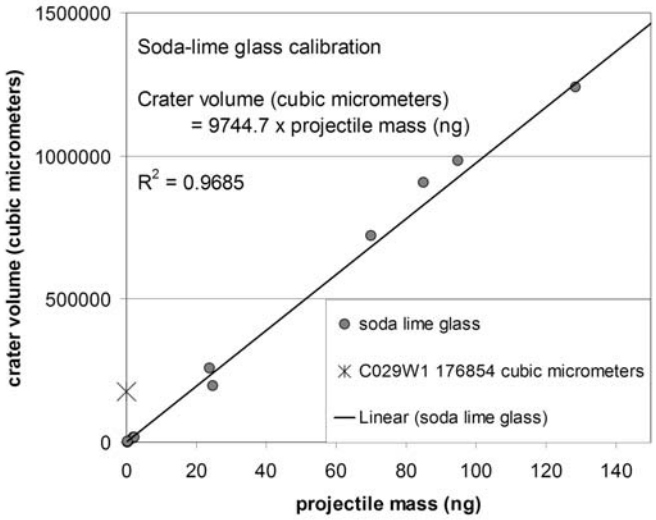

Fig. 4. Plot of experimental impact crater size (displaced volume of Al, measured internal to crater, below pre-impact surface as seen in MeX DEM) as a function of soda lime glass projectile mass (ranging from 0.2 ng to ~130 ng, calculated from measured crater top-lip diameter, using the diameter relationship of Kearsley et al. (2006), and a density of 2.4 g cm^{-3}). The volume of the large compound crater on Stardust foil C029W,1 is shown as a cross on the Y-axis, corresponding to inferred particle mass of ~18 ng when extrapolated to intersect the linear plot.

show relatively simple plan view outlines (close to circular) and "bowl-shaped" depth profiles (Fig. 1) of De/Di ~ 0.56 to 0.81. Some of the craters contain residue that is almost entirely derived from a single mineral species, whereas others show a mixture of compositions, probably reflecting diverse mineral (and/or amorphous) species within the impactor (Kearsley et al. 2008a). The precise compositional range of residue has not yet been determined, partly due to geometrical problems with extraction of focused ion beam (FIB) sections from these relatively deep, narrow craters. The similarity of the simple bowl crater shape to experimental impacts by single-crystal silicate impactors led to an initial assumption that the cometary dust grains probably had similar bulk density and little internal porosity (Kearsley et al. 2008a). Our new experimental data from large aggregate impacts now allow us to make a better comparison.

Two larger Stardust craters show complicated and shallower depth profiles, interpreted as evidence of impact by lower density aggregates. One particularly complicated (compound) crater on foil C029W,1 shows diverse residue compositions within separate modified bowl depressions, implying an aggregate of different mineral sub-grains (Kearsley et al. 2008a). A simple model of the component sub-grain dimensions was inferred from the location and rim diameter of crater arc-segments, and was combined with likely density values (based upon X-ray microanalyses of the impact residues) to yield an estimate of overall particle mass, porosity and density (Kearsley et al. 2008a). The volume of foil metal displaced by this impact event has now been measured from a MeX DEM as ~1.8×10^5 μm^3. Several previous experimental studies of micro-cratering (Rudolph 1968; Eichhorn and Grün 1993) have shown that, where the target dimensions are "semi-infinite" (i.e., allow the cratering process to run to completion before a material boundary can be reached), there is a linear relationship between kinetic energy of the impactor and the volume of target material displaced. In our earlier particle size calibration experiments (Kearsley et al. 2006), we used well-constrained projectile and target materials, and a narrow impact velocity dispersion, and can therefore generate a volume-displacement calibration plot for monodisperse soda lime glass bead samples (Fig. 4), which confirms the linear relationship. When mass estimates from the simple model are compared to a value derived from the measured volume displacement, similar results are obtained (19 ± 3 ng : 18 ng, respectively).

A hydrodynamic numerical simulation of this impact was performed at the University of Kent, using AUTODYN 3D. Values of size, mass, equation of state and spatial distribution suggested by the simple model described above were applied to the individual sub-grain components. The result (Fig. 5b) is highly informative, reproducing the broad outline shape of the structure including internal pits and septa, but also revealing that improvements could be made to some of the inferred particle masses and spatial distribution (particularly in the third, line-of-flight, dimension). Refinements to this simulation are currently in progress, but even the first iteration supports interpretation of this feature as the product of impact by a very porous aggregate of low density.

The compound crater on foil C091W,1 (Figs. 5d, 5f) shows a rather different depth profile to the classic simple bowl shape, apparently consisting of two closely superimposed sub circular craters, one cutting and almost entirely reworking the rim of the other. The floor of this feature also appears flat rather than a curved bowl, and the associated DEM reveals superimposed smaller depressions on the floor of the larger structure.

Smaller Stardust impact structures exhibit a great variety of plan-view outline and three dimensional complexity in stereo-pair images and digital elevation models (Fig. 5). From the small number so far reconstructed as DEM by MeX, it appears that few have simple bowl-shaped depth profiles, most show overlapping and mutually interfering depressions. However, even cursory examination shows that few of the smaller craters are as shallow in relation to their width as the compound crater described above, and most show relatively deep, overlapping depressions. Nevertheless, where energy dispersive X-ray microanalysis has been performed on small craters (either in situ in unprepared craters, or by TEM of FIB-cut sections), residues of several different compositions can be found together, implying polyphase impactors (Kearsley et al. 2008; Leroux et al. 2008b), often with crystalline remnants of a substantial proportion of the impactor, without clear evidence of non-stoichiometric amorphous materials.

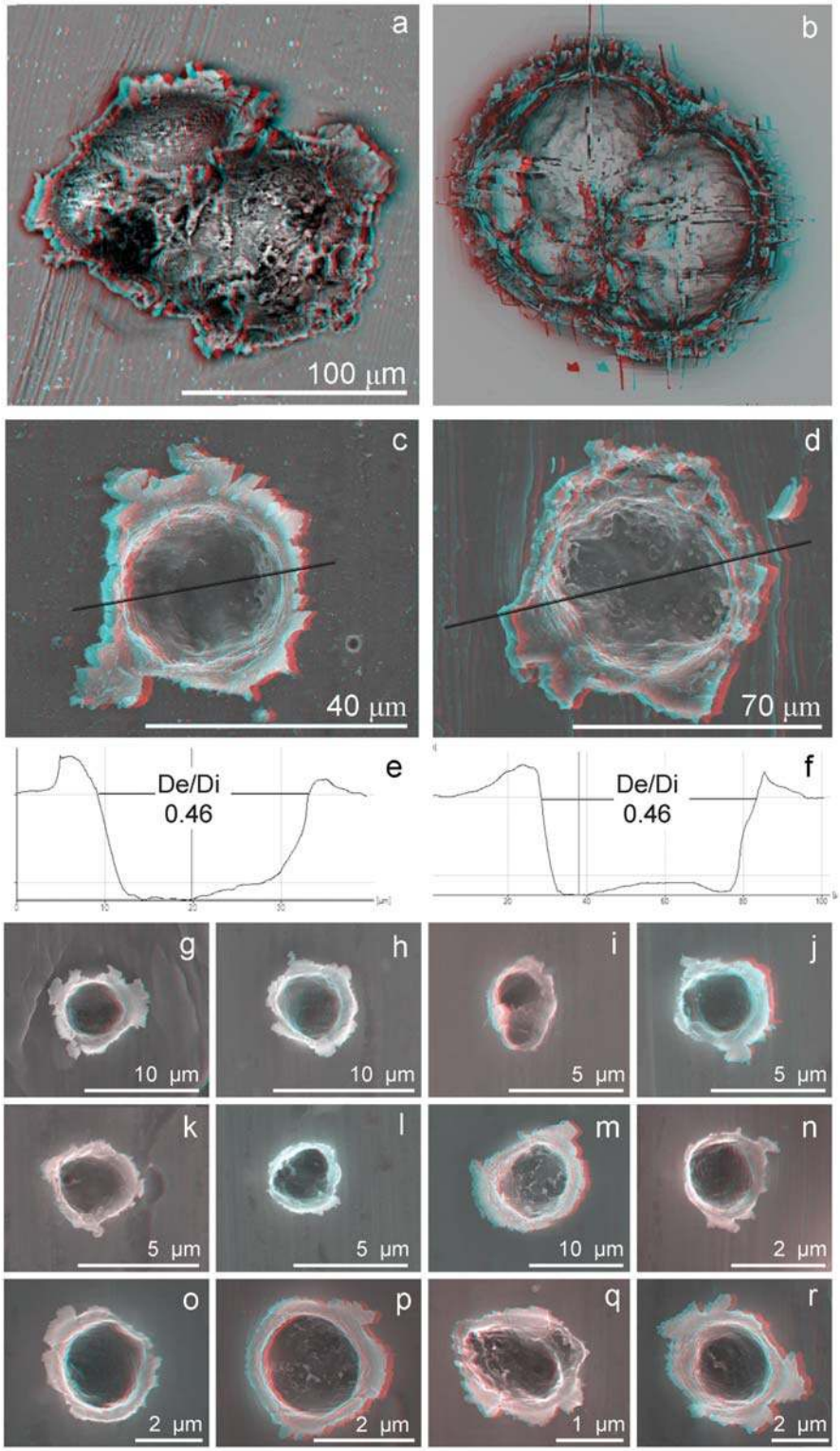

Fig. 5. Stardust foil impacts, stereo anaglyphs (left eye red, right eye green). Comparison of the large compound crater on Stardust foil C029W,1 (a, SEI) with an AUTODYN 3D simulation (b), based upon the model of particle internal structure ascribed by Kearsley et al. (2008a). Comparison of stereo anaglyphs and MeX depth profiles of compound craters: formed by impact of a dense, polymineralic, artificial aggregate containing impact residue from diopside and pyrrhotite (c and e); with a Stardust crater on foil C091W,1, containing Mg-rich silicate and Fe-sulfide residue (d and f). Despite difference in overall scale, the similarity in general form probably reflects a similar relationship of sub-grain to entire impactor size. Stereo anaglyph SE images of smaller Stardust craters (g to r), all on foil C011N,1. Note the wide range of subsurface three dimensional shapes, few being truly "bowl-shaped."

RESULTS FROM LABORATORY EXPERIMENTS

Low-Density Polydisperse Aggregates

The shots of olivine, enstatite and polymineralic aggregates onto Al 6000 series each yielded a few small compound features. Some of the polymineralic impactor craters contained residue derived from more than one mineral component, as illustrated in Kearsley et al. (2008b). The majority of impact features on the stub surfaces were simple craters of a wide size range, but with each only containing residue from a single mineral component.

Low-Density Lizardite Aggregates

The shot of polydisperse lizardite aggregates onto Al 6000 series generated few larger impacts, but a large number of small compound craters (Fig. 6 top), in contrast to the targets from other low density polydisperse aggregate shots.

Higher-Density, Monodisperse Fine Olivine Aggregates.

The first shot (G210208#2) gave very few impacts on the target, but the second shot, using projectiles from the same production batch, yielded a target peppered with many thousands of impacts, from sub-micrometer to sub-millimeter scale (Fig. 6). A much higher proportion of the impact features were compound impacts than were found in shots of the low-density aggregates. The smaller craters (μm to 20 μm) vary greatly in shape, with most being compound, and many showing irregular outline morphology similar to small Stardust craters, with multiple bowl overlaps (Fig. 6, lower). There are numerous "clusters" of small irregular craters (Fig. 6, lower) like those reported from Stardust. The relatively deep internal depressions are also similar in shape and size to those of Stardust. Most of these craters contain abundant residue of high magnesium and silicon content, recognizably derived from olivine. A few very shallow craters (De/Di ~ 0.25) of oval or irregular external outline, yet lacking complicated internal septa, show no obvious residue but have a distinctive polygonal surface cracking on the crater floor.

Most intermediate scale craters (20 to 50 μm) are sub-circular in top-lip plan view, although with more complicated internal shape apparent in stereo anaglyphs. The small to medium-scale experimental craters will be the focus of intensive study by FIB-TEM, particularly regarding the preservation of crystalline remnants and generation of apparently amorphous materials.

The numerous larger impacts (>50 μm diameter) have relatively circular outlines and simple bowl-shaped profiles (Fig. 7). Their abundance is not consistent with the low level of coarser olivine grain contamination in the projectile powder (<0.3%) and we attribute these impacts to stronger, large aggregates. The De/Di determined from MeX DEM reconstruction averages at 0.54 (n = 27, Std. Dev. 0.07) as compared to that for single grain olivine impacts which we determined previously as 0.71 (Std. Dev. 0.08). Together with evidence from our imagery of polished aggregate cross-sections, yielding an estimated aggregate density of ~2.4 g cm^{-3}, these craters define a plot position offset below that of single mineral, dense olivine (Fig. 8).

Higher-Density Monodisperse Polymineralic (Olivine/ Diopside/Pyrrhotite) Aggregates

The first shot (G221208#1) of aggregates with rather poorly mixed sub-grains yielded only a few impact features on the target. Although most were compound craters, their residues suggest that the sub-grains of each impactor were composed of only a single mineral species. However, one feature (Figs. 5c, 5e, and 9) contained residue with markedly different compositions across the crater, and although dominated by diopside-derived residue, some patches are low in Ca and high in Mg (suggesting a contribution from the olivine), and a diffuse presence of sulfur suggests that sub-micrometer residues from pyrrhotite are widely distributed throughout. A second shot (G221208#2) onto aerogel generated numerous Type C bulbous tracks, including one large example (Fig. 9g).

Meteorite Powder Impacts

The craters produced by carbonaceous chondrite powder projectiles also show variation in shape, with larger craters again being simple bowls, while smaller craters (of <50 μm diameter) are often complicated in internal form (Fig. 10). The small compound Allende craters (Fig. 10 top) are dominated by Fe-rich silicate residues (and rarer Ca-rich silicates), whilst compound Orgueil craters (Fig. 10 bottom) may contain mixed Fe, Ni, Mg, Si, O and S rich-residue and patches of Fe oxide or Fe sulfide. We have not, however, observed clustering of craters, or shapes so complicated as those produced in our artificial aggregate particle shots.

DISCUSSION

Our previous work (Kearsley et al. 2007, 2008a, 2008b) has shown that LGG impacts by single mineral grain projectiles at ~6 km s^{-1} usually yield craters with a simple, near-circular plan outline and "bowl-shaped" depth profile. Impactor shape may play an important role if the grain has a markedly inequant shape, as impacts at varying angles of pitch (relative to the long axis) will generate different crater circularity and crater depth (Kearsley et al. 2008b). For example, our shots of angular olivine shards (Fig. 5 of Kearsley et al. 2008a) do not create the very wide range of crater De/Di seen in impacts by acicular wollastonite needles

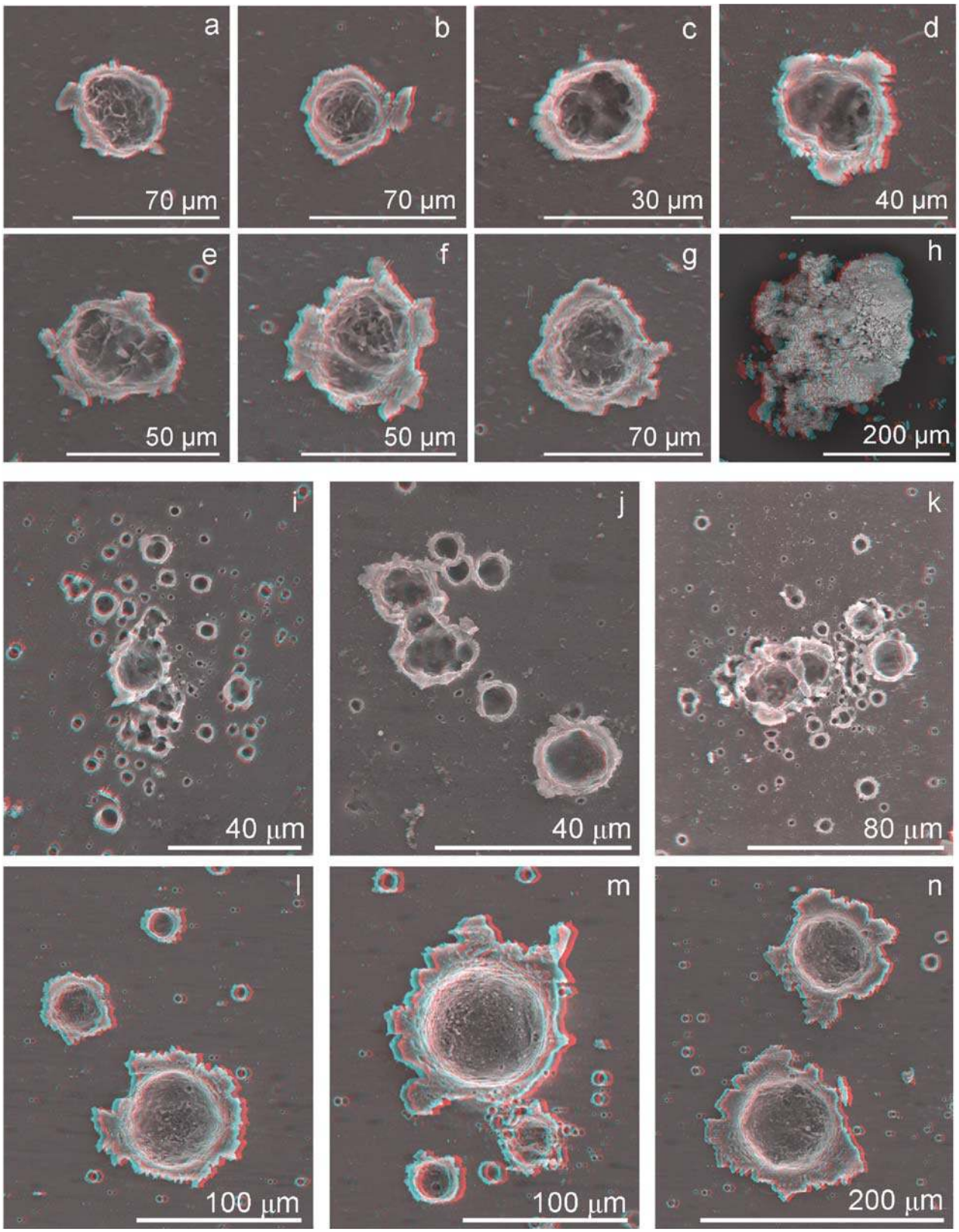

Fig. 6. Stereo anaglyph SEI of experimental impacts on Al1100 foil by: monomineralic, polydisperse low density, high porosity lizardite aggregates (craters a to g, aggregate projectile h); and monomineralic, monodisperse, high density, low porosity, fine olivine aggregates (craters i to n). Note compound shapes for smaller craters (10–50 µm, and bowl-shapes for larger craters (>50 µm), flatter bases may reflect near penetration of the foil thickness.

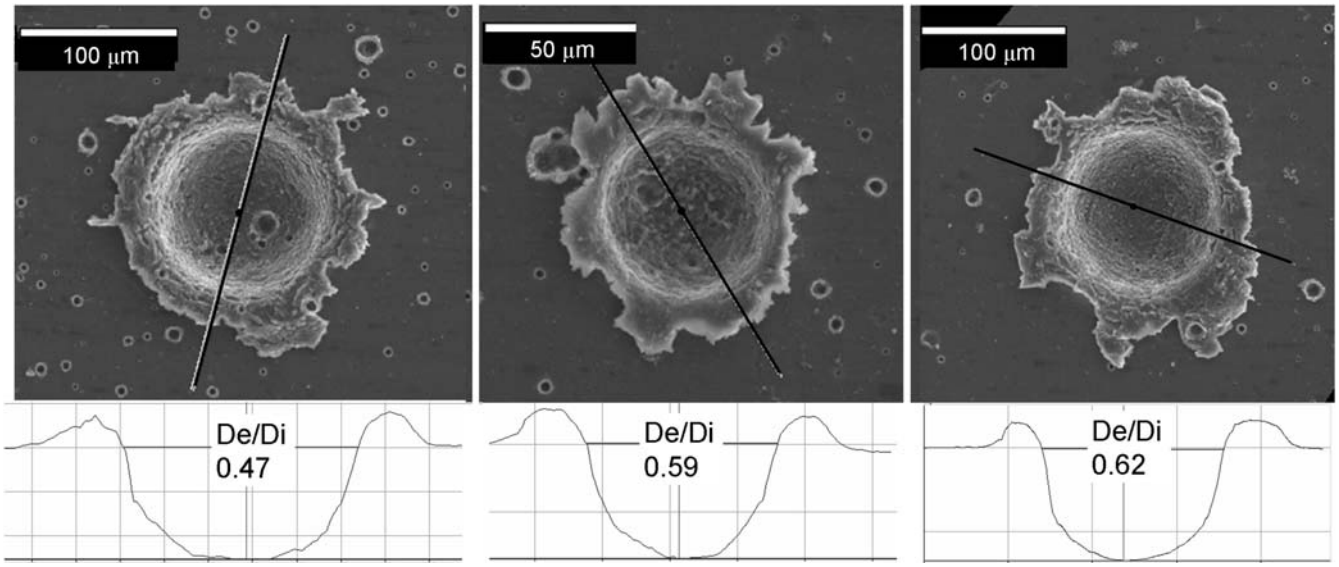

Fig. 7. Top: SEI of typical impacts by large aggregates made from fine-grained, monodisperse olivine. Bottom: Depth profiles of the craters generated from MeX DEM, labeled with De/Di.

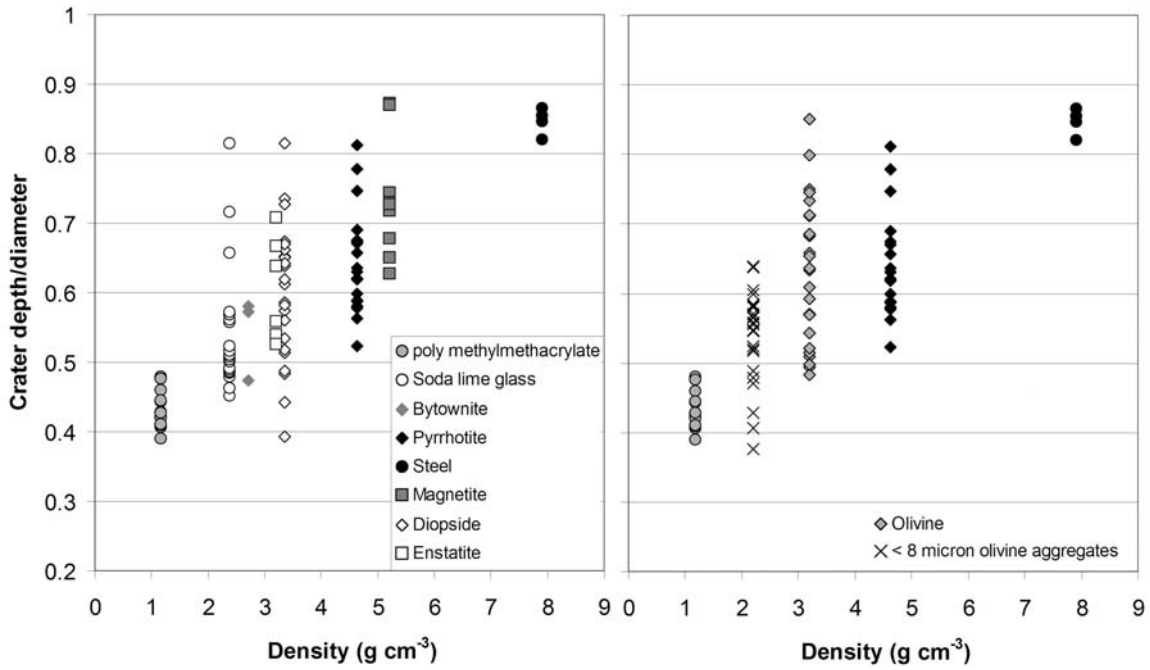

Fig. 8. Left: Impact crater depth/diameter as a function of projectile density; measurements from LGG shots of monodisperse glass, polymer and metal beads and polydisperse monocrystalline mineral powders (revised from Kearsley et al. 2008b, with addition of new mineral data). Dispersion of soda lime data is due to fragmentation into small angular shards during firing. Right: Plot of De/Di for large bowl-shaped craters formed by mid-density monomineralic aggregates of monodisperse olivine, compared to single-crystal, dense (~3.2 g cm^{-3}) olivine grains.

(0.26 to 0.97; Fig. 21 of Kearsley et al. 2008b), suggesting that projectile shape factor (aspect ratio) must be very high for major influence. Where particle shape is more equant, impactor density seems to control average depth/diameter (Kearsley et al. 2008b), with higher density particles (e.g., steel) creating relatively deeper craters than, for example, low density polymer grains. Although complex impactor shape can complicate matters, the average depth/diameter of experimental craters made by homogeneous, non-porous grains is clearly linked to their bulk density. The range of De/Di ratios is now becoming well documented and, even with the data dispersion evident in Fig. 8, it is clear that many artificial aggregates of fine olivine produce shallower craters than single-crystal olivines of equivalent diameter. Where the sub-grain dimensions are a small fraction of the overall particle size (i.e. in our bigger aggregates of monodisperse

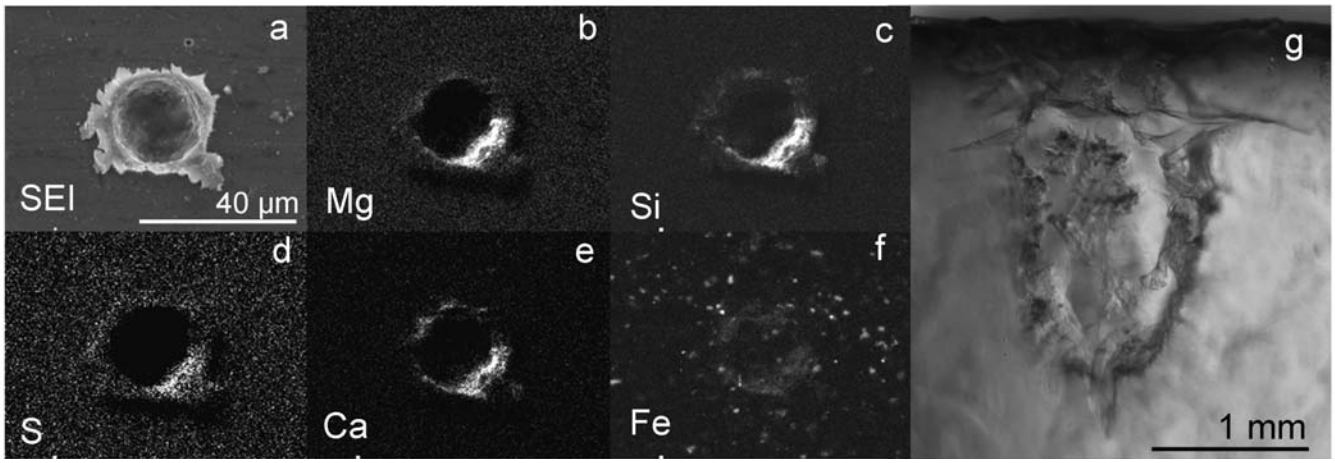

Fig. 9. Experimental impacts by polymineralic monodisperse, high-density, low-porosity aggregates: at left on Al foil, SEI and X-ray maps (Mg, Si, S, Ca, and Fe); at right, forming a Type C bulbous track on aerogel.

olivine), the aggregate behaves as though it were an almost homogeneous, albeit low density, particle and creates a bowl-shaped crater. If sub-grain dimensions are a larger fraction of the whole (i.e., smaller aggregate fragments), each sub-grain exerts influence on the development of crater shape, and more complicated craters are formed. If we assume that the bulk density of our bigger olivine aggregate projectiles is ~2.4 g cm^{-3} (similar to soda-lime glass) then a 10 µm projectile might be expected to have an internal construction with between 3 and 10 smaller grains across its width. Craters of ~50 µm, produced by such aggregates, lie at the threshold for change from compound to simple-bowl morphology. It appears that if an aggregate is less than 3 to 10 times larger than the dimensions of its constituent sub-grains, it is likely to produce a compound crater morphology. In the case of individual meteorite powder projectiles (which do produce some compound craters), we cannot directly constrain the internal structure and composition of each impactor. However, compound Allende craters usually contain residues with compositions resembling the characteristic iron-rich olivines that are so common as an open framework of laths of a few micrometers in grain-size (typically ~2 µm long axis) making up the porous Allende matrix. In the case of Orgueil, the explanation for compound crater morphology may not always be so simple. Polished sections show that the meteorite contains two populations of grain size: very fine-grained (<<µm) hydrous silicates; and coarser (>µm) grains, mainly Fe oxides and sulfides. The residue within the compound craters suggests an origin from either a mixture of these phases (in a few craters), or solely from the phyllosilicates. In the latter case it may be that there are differences in density on a scale of a few micrometers, reflecting extremely fine scale porosity variations, which are not resolved as discrete pores in BEI of the projectile material, but are suggested by subtle grey tone variations across areas greater than micrometer.

For interpretation of the range of morphology shown by small but complicated Stardust craters two other factors must also be considered. First, it is possible that there could be a bias in the recognition of small crater shapes due to the surface irregularity of the Stardust foils and the methodology used to recognize impact features. The foil surface shows ridges and furrows with topographic expression of micrometer scale, uplifted pits with radial tension gashes around Fe-oxide inclusions, and a variety of abundant surface indentations and scratches. Many of the indentations have very irregular shapes, but occur in extensive linear strips, suggesting formation by mechanical contact during assembly prior to launch, and they can thus be discounted as hypervelocity impact features. However, during the search for small craters, the primary criterion for recognition of an impact generated structure is usually the appearance of a bright SEI "edge-effect" marking the uplifted crater rim. Such a prominent feature is best developed around a deeper bowl-shaped feature, and it is possible that detachment of a very thin metal lip might leave only a poorly defined uplift zone around a small compound crater, or even a partial surface "skin detachment" (as shown in the very small craters of Kearsley et al. 2008b), removing the most obvious evidence for hypervelocity impact origin. The quantity of impact residue is also likely to be very small from a tiny aggregate, and preserved as a thin film (of only a few tens of nanometers thickness). Given the known heterogeneous impurities in the foil, especially the localized Fe and Si concentrations (Kearsley et al. 2007), and the common silica aerogel particulate contamination which can become lodged within surface irregularities, it is very difficult to distinguish impact residue without recourse to sophisticated surface analysis techniques (e.g., Auger spectroscopy, Stadermann et al. 2007) whose speed and expense are impractical for large area characterization. Electron beam scattering within small craters can also yield a misleading impression of the distribution of "residue," with X-ray emission from

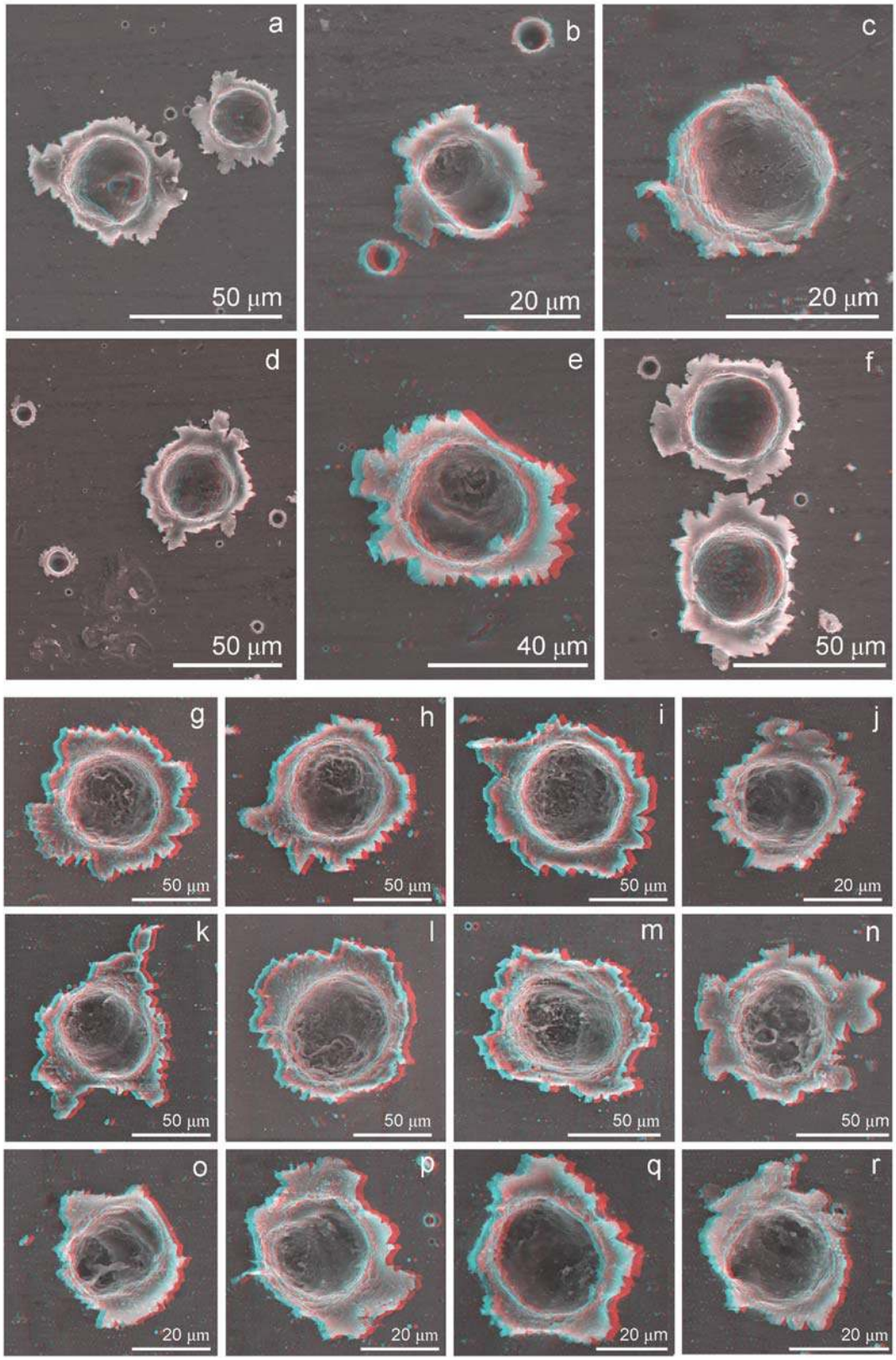

Fig. 10. Stereo anaglyph SEI of craters formed by laboratory impact of powdered carbonaceous chondrite meteorite projectiles, fired onto Stardust Al foil: Allende projectiles, images a to f; Orgueil projectiles, images g to r.

localized residue, or contaminants, being stimulated by spot irradiation even at a distance of several micrometers. There is therefore a real possibility that the number of small, shallow and complicated impact features on Stardust foils has been underestimated.

A second complication arises in the possibility of impacts by secondary ejecta from cometary dust impacts on other parts of the spacecraft. Our recent, as yet unpublished, laboratory experiments to simulate generation of secondary ejecta from the spacecraft solar panels behind the collector, show that irregular droplets of molten materials splashed at a high angle from the primary impact site may also generate compound crater morphology when they impact onto a second surface such as Al foil. Their lower velocity usually results in shallower impact features with poorly uplifted rims. Fortunately, they also contain abundant residue from the solar cell components (easily recognized by a distinctive composition), and the surrounding surface is also usually embedded with abundant solid fragments of ejecta, neither of which have been found on Stardust cometary collector foils. It is therefore unlikely that the cometary foil crater clusters were formed by ejecta from solar cell arrays. Were they created by debris from impact onto low density Kapton (~1.4 g cm^{-3}) in the multi-layer insulation (MLI) foil blankets on the Whipple Shield in front of the collector, as discussed by Westphal et al. (2008)? In our experience, organic materials do not give a well-preserved hypervelocity impact residue and hence any associated Kapton secondary ejecta, although likely to yield very shallow craters, would be difficult to recognize on the foils. The abundant small craters on foil C011N,1 (from within an area of clustering described by Westphal et al. 2008), are quite deep (Fig. 5, bottom), and all seem to contain Mg-silicate residue. They show more complicated 3D shapes than simple bowls, and were probably formed by fragments that were still solid aggregates. Graham et al. (2003) have demonstrated that crystalline (i.e., solid) olivine can survive perpendicular LGG impact onto Kapton MLI foils at 5.1 km s^{-1}, and we therefore suggest that the creation of these craters could indeed be the result of grazing contact by a larger cometary dust grain onto a curved surface of thin Kapton foil, an impact which did not exceed the melting temperature of the aggregate components, but generated a narrow sub-conical debris cloud, propagated down-range to impact the Stardust collector. Were almost all of the smaller Stardust craters made in this way? Stereo imagery and three dimensional reconstruction of shape has not yet been carried out for more than a few of the small craters found at a distance from the spatial clusters. Some of those found during the Stardust PE were more complicated and shallow (e.g., on foil C125N,1; Kearsley et al. 2008b; Fig. 15), and perhaps do record a few impacts by pristine, small, very fine-grained, porous aggregate grains of low density. The residue composition within about half of the smaller (<20 μm) craters examined during Stardust PE indicates both silicate and sulfide components together (Kearsley et al. 2008a), even within dust of micrometer scale. Sections of a few micrometer-scale craters have been examined by TEM (Leroux et al. 2008b). Some show quite coarse crystalline mineral remnants (>100 nm) and patches of similar homogeneous composition (probably shock melt), implying that the original particle was probably not composed of nanometer-scale grains or rich in amorphous material. We suggest that more FIB sections should be made from small Stardust craters, to establish the homogeneity of composition in the residues, and that better understanding of the crater forming process and residue preservation, involving both experimental work and numerical modeling, will be required to help interpret these craters.

In LGG shots of aggregates, artefacts which could be confused with aggregate impacts also occur. As well as mineral-bearing aggregates, coarser fragments of the solidified adhesive binder, and even debris from the nylon sabot, may also reach the target foil and create shallow impact features. Fortunately, the distinctive "crazed" polygonal surface texture within craters formed by impact of organic projectiles (as seen in our impacts of poly methylmethacrylate spheres) makes them easy to recognize, despite their lack of evident carbon-rich residue.

As mentioned earlier in this paper, the nature of cometary dust not only influences the shape of craters in the Stardust aluminum foils, but also that of the tracks in the aerogel. We assume that the large craters and large tracks on the Stardust collector were created by the same population of impactors and, with our new experimental evidence, we can begin to suggest a combined taxonomy (see Fig. 11). The three aerogel track types A, B, C (see Hörz et al. 2006; Burchell et al. 2008), were held to reflect respectively: well consolidated grains (whether monocrystalline or very compact, strong, dense aggregates), mixtures of well consolidated material with volatile rich/loosely bound smaller sub-grains, and finally just assemblages of volatile-rich and/or loosely-bound small sub-grains. In parallel, these three types of impactor are considered to produce: deep bowl-shaped craters (e.g., Fig. 1), shallow bowl-shaped craters with internal complexity reflecting sub-grain dimensions (e.g., Fig. 6); and very complicated, shallow features (Fig. 5), respectively. The large simple-bowl craters created by our strong olivine aggregates are >50 μm in diameter (many are 80–100 μm, see Figs. 6 and 7). By comparison to our previous calibration work (Kearsley et al. 2006) we infer that this is 4 to 5 times larger than the impactor diameter, implying particles of 10 to 20 micrometers in size. Experimental data from Burchell et al. (2008) show that aerogel tracks created by single-crystal or other very robust particles of this size would usually create tracks of type A. Although we do not yet have results from many laboratory impacts onto aerogel by experimental aggregates, we have already observed that small Type C tracks are created by monodisperse fine-grained aggregates, in contrast to the Type B tracks made by lizardite powder (Foster et al. 2008), a

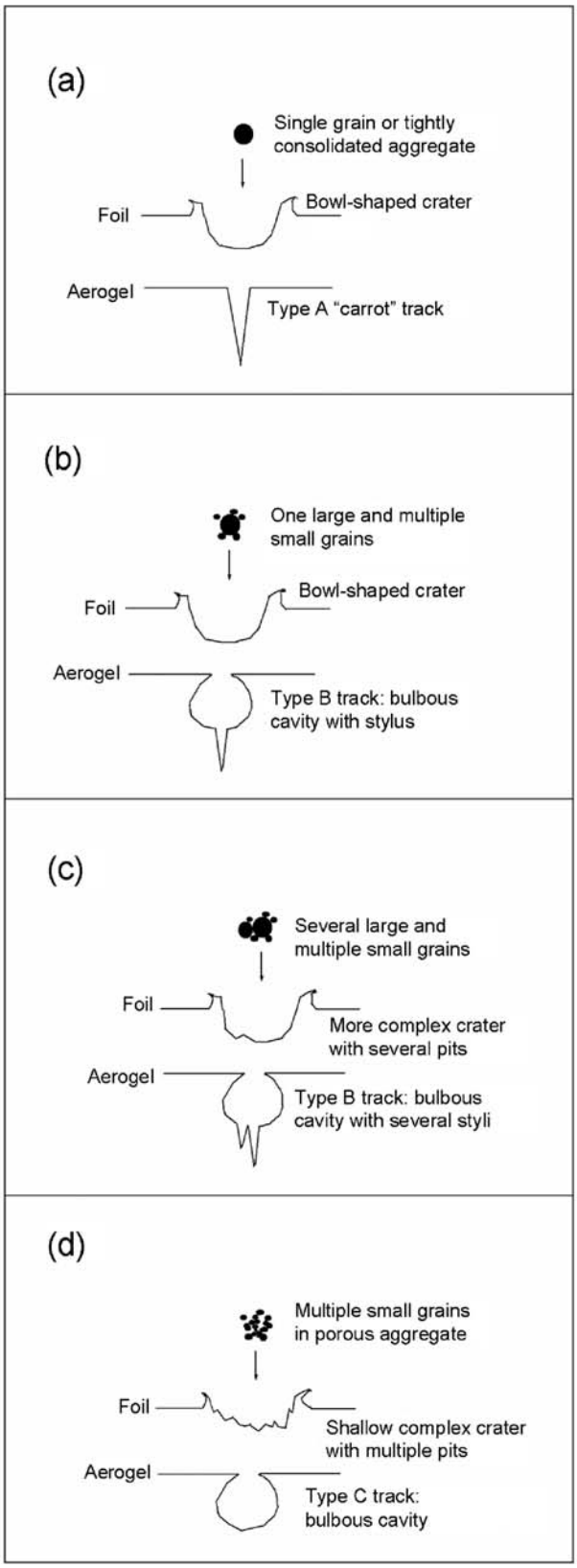

Fig. 11. Taxonomy of impact crater and aerogel track morphology related to particle structure.

projectile material which SEM images reveal is made of natural porous, polydisperse aggregates (Fig. 22 of Kearsley et al. 2008a)

Burchell et al. (2008) noted the frequency of each track type in the Stardust aerogel: only 2 % of tracks were Type C; overall the ratio A/B was 2:1, but the A/B split had a strong particle size dependence; 100 % of tracks for sub-micrometer sized impacting particles were of Type A, while 90% of the tracks from particles >20 μm were of Type B, with a gradual transition at intermediate sizes. For large impacts, the dominance of type B aerogel tracks on the Stardust collector implies that the majority of large dust particles were not simply robust or monocrystalline particles, and the paucity of type C tracks indicates that weakly bound assemblages composed of many fine-grained particles were also relatively rare. By contrast, the interpretation of the larger Stardust craters (4 of 7 large craters) as bowl-shaped, suggests the particles were well-consolidated, containing either a coarse single mineral grain (possibly accompanied by a quantity of fine-grained loosely bound components), or in the somewhat shallower examples, a relatively high density aggregate with many sub-grains. We also note the observation (see Fig. 16, Burchell et al. 2008) that 43% of type B tracks have just 1 stylus underneath the initial bulbous cavity (35% have 2 stylii, 15% 3 styli and only 6% have 4 or more styli). We therefore suggest that the majority of larger Wild 2 dust grains were aggregates, albeit compact and relatively strong, containing relatively few distinct large sub-grains. A large particle with >10 loosely bound components with no single dominant grain, may well give a type C bulbous aerogel track or a compound, shallow crater in the foil, but such features seem relatively rare.

With the smaller craters and tracks the situation is less clear. The small cometary particles in Stardust gave predominantly type A aerogel tracks, but the small craters can have a complicated morphology. However, Price et al. (2009) have reported that experimental craters from impacts of small (less than 10 μm) particles on Stardust foil do not scale as expected from observations of larger particles, indicating a less efficient cratering process. The mechanisms of crater formation by small cometary dust require further study before we can reliably interpret the structural nature of the smallest particles. Here we tentatively suggest that sub-micrometer particles may produce craters more sensitive to particle shape effects, or that the single grains (Type A tracks) may be well-consolidated (internal strength sufficient to survive ~1 GPa shocks), but of more than one mineral (e.g., similar to components of the particle "Febo" shown in Fig. 2 of Brownlee et al. 2006), with the combination of different density components influencing crater shape, but producing only Type A aerogel tracks. Higher resolution compositional imaging of the smaller aerogel tracks, combined with an improved understanding of cratering at sub-micrometer scales, may help to resolve this issue.

CONCLUSIONS, IMPLICATIONS, AND FURTHER WORK

Although the near-circular plan outline and De/Di of the deeper "bowl-shaped" Stardust craters (e.g., Fig. 1) are similar to laboratory craters produced by single-crystal, low-porosity silicate projectiles at ~6 km s^{-1} (Kearsley et al. 2008b), we have now shown that big bowl-shaped craters can also be produced by impact of large fine-grained aggregate particles of intermediate density (~2.4 g cm^{-3}), and by powders from meteorites with 20 to 35% bulk porosity. The depth profile of these aggregate craters (Fig. 8) lies at the lower limit for shallower Stardust bowl-shapes (see Kearsley et al. 2008a), implying that most Wild 2 grains were higher in density, and 2.4 g cm^{-3} is probably the minimum attributable to the majority of large Stardust grains i.e., those carrying most of the cometary dust mass. If the Stardust grains are assumed to contain predominantly mafic silicate, sulfide and unfilled pore-space, although the presence of organic material has been demonstrated in some (Leitner et al. 2008), this would imply that the uppermost limit for porosity in "bowl-making" grains is ~25%, much lower than the 75% porosity (Kearsley et al. 2008) estimated for the aggregate which created the extraordinary feature on foil C029W,1 (Fig. 5 a).

With the recent discovery that there may be lower crater excavation efficiency for micrometer-scale grains (Price et al. 2009), our comparison between the shape and scale of experimental aggregate impact features implies that most of the dense individual component sub-grains of Wild 2 fine dust responsible for the craters in Fig. 5 were probably around to 0.5 to 5 micrometers in size, although a small proportion may have been as small as 100 nm. Even smaller, sub-micrometer craters abound in the samples examined during Stardust foil PE, many appear to be irregular in outline but also deep, suggesting they too were made by dense aggregates composed of still smaller sub-grains, perhaps a few tens of nm in size. Thus evidence from a very wide range of crater sizes indicates that the majority of Wild 2 dust is clearly not made of very low-density, highly porous fractal aggregates of nm-scale sub-grains, although it is composed of a mixture of materials.

What does the presence of dense aggregate structure tell us about the origin of Wild 2 dust, and its subsequent evolution? It is important to consider our structural interpretation in the context of evidence from aerogel-captured particles. Unfortunately, the relatively poor preservation of micrometer and smaller particles in aerogel (Ishii et al. 2008) makes them difficult to interpret. Although the major element composition of small areas on the walls of large aerogel tracks may resemble that of bulk chondritic meteorites (Leroux et al. 2008a; Stephan et al. 2008), it is not yet proven whether these are remnants of sub-micrometer scale amorphous dust, or mixed impact residues from several different (possibly even crystalline) components, spattered and partly dissolved into high-temperature silica melt. The chemical composition of these fine patches is therefore not an unequivocal indicator of IS or DMC particle types (Zhukovska et al. 2008) as might be expected to be fractal grain cores in the model of Greenberg et al. (1989). Our interpretation of the finer dust structure and density definitely does not fit with the simple Greenberg et al. model, nor does the frequent presence of stoichiometric and crystalline material in micrometer (and smaller) Stardust craters (Leroux et al. 2008b) which, by analogy with residues from our experimental impacts of minerals, we regard as an indication of crystalline structure in even the smallest dust particles, known from isotopic studies (Stadermann et al. 2008) to be equilibrated solar system material. Thus, if the Greenberg et al. model is an accurate representation of primitive pre-nebular dust derived from IS or DMC sources, such material has probably not survived as an abundant component of comet Wild 2.

Does the dense aggregate structure therefore represent well-preserved first-generation "agglomerates" of nebula-processed dust, made by the mechanisms summarized in Blum and Wurm (2008)? The diverse range of minerals with unequilibrated elemental compositions reported from particles in Stardust aerogel tracks (Zolensky et al. 2008), most showing evidence of pervasive isotopic equilibration (McKeegan et al. 2006), has indeed been interpreted as an indication of extensive nebular processing involving high temperatures (Brownlee et al. 2006), which must have occurred prior to mixing with the more volatile cometary components i.e., ices. However, the internal structure of some grains is reminiscent of chondrule textures (Nakamura et al. 2008), suggesting melting of millimeter-scale dust aggregates. Unfortunately, without knowing the detailed contact relationships between individual sub-grains in most impactors (textures that our experiments show are always destroyed during impact on foil and in creation of bulbous Type C aerogel tracks), we cannot directly assess the mechanism by which the different components became associated, whether mechanical ("sedimentary") or by crystallization from melt ("igneous"). Nevertheless, the overall high density and low porosity of the particles provides an important clue. The elegant microgravity experiments described by Blum and Wurm (2000) show that low velocity particle collisions in low pressure gas create primary fractal agglomerates of micrometer scale grains, with an open framework structure, very low density and high porosity. This process is likely to be important in the earliest steps of larger scale mechanical accretion of solid particles in the nebular disk, being repeated whenever fine-grained materials encounter the correct conditions. Our particle structure again does not resemble these agglomerates, and we therefore suggest that Wild 2 dust does not preserve the earliest nebular grain accretion textures.

How then did relatively dense compact aggregates come into being? Whole track synchrotron X-ray maps show that many Type A Stardust aerogel tracks contain dispersed remnants of multi-component particles, although they are only occasionally physically intact (e.g., particle Febo, Brownlee et al. 2006). Usually their internal structure is disrupted or modified by intrusion of aerogel, and again we cannot use texture to reliably evaluate the proportion of particles formed by crystallization from melt, as opposed to mechanically-assembled "sedimentary" aggregates. However, the diverse, co-existing compositions are sometimes difficult to explain as mutually equilibrated "igneous" assemblages. For example, the large and relatively deep crater on foil C086W,1 (which we interpret as formed by a dense particle) contains diverse residue major element compositions (Kearsley et al. 2008a) similar to those seen in shots of carbonaceous chondrite powder. Stadermann et al. (2008) showed that this crater contained both equilibrated solar system material and at least one isotopically anomalous presolar grain, and it therefore seems likely that the impacting particle was a "sedimentary" aggregate. In another example, the differing range of iron and magnesium ratios seen in the olivine and pyroxene grains in aerogel track 17 described by Zolensky et al. (2008) could be interpreted as the result of separate sub-grain origins from different sources, brought together by large scale mixing (e.g., Ciesla 2007), and then mechanically aggregated. In both of these examples the particles clearly had relatively high density, not the loose packing of an open framework (c.f. Blum et al. 2006), implying significant post-accretion compaction.

Although impact into aerogel itself damages the captured grains, the rarity of distinctive and pervasive solid-state shock features (e.g., Tomeoka et al. 2008) and absence of pre-capture melt veins or small scale vaporization in the larger Stardust particles, together argue against a high velocity impact mechanism for the majority of dust grain accretion and compaction. There is also little evidence of extensive aqueous parent-body processing (Zolensky et al. 2008), which might be expected if compaction of a cometary dust and ice mixture in the regolith of a major body were driven by major impacts (Trigo-Rodríguez and Blum 2009). Blum et al. (2006) and Ormel et al. (2007) have shown that low velocity (~1 m s^{-1}) impact compaction of mineral dust aggregates yields only relatively low volumetric packing efficiency (VPE), <15%, and hence high porosity and low bulk density. Rates of growth and fragmentation reach an equilibrium, limiting compaction in small mineral aggregates, and impact velocity only reaches a sufficient level to promote compaction beyond 30% VPE when aggregated protoplanetesimals reach meter size. However, recent experiments by Weidling et al. (2009) demonstrate that cm-scale aggregates can be compacted to 30% VPE by impacts at velocities predicted in and around the nebular mid-plane environment, as previously postulated for the consolidation of fine chondrite meteorite matrix by Wasson (1995). Our comparison of experimental impacts and Stardust samples strongly suggests that some Wild 2 dust compaction went further, creating even denser aggregates containing polydisperse grain mixtures with diverse mutually-unequilibrated provenance, before mixing with ice. Whether early incorporation of organic matter may have played an important role in providing greater internal strength (aiding the survival and hence compaction of fine aggregates) is unknown. Our observation of greatly enhanced survival in the extreme acceleration of light gas gun shots when artificial aggregates are acrylate-bonded hints that this may be an important factor. How large the compacted bodies became, the dynamics of their scattering, and the mechanisms of disruption before partial mixing with volatile icy materials remain to be discovered. However, the low bulk density of the Wild 2 nucleus (0.6 to 0.8 g cm^{-3}; Davidsson and Gutièrrez 2006) indicates that even with a high proportion of low density ice, there must still be abundant open pore space between aggregates (and ice), implying very limited compaction after accretion of the nucleus, and no significant impact-generated mineralogical alteration. The internal structure of Wild 2 therefore probably differs from the stratiform model proposed for comet Tempel 1 (Belton et al. (2007), with the bulk mechanical properties possibly being responsible for the differences in surface appearance.

Whether mechanical compaction alone generated sufficient strength for aggregates to survive eventual ejection from the nucleus of Wild 2 and into the coma is unknown. Prolonged but intermittent disaggregation of aggregates during motion across the coma has been implicated by both a non-random spatial distribution of clustered impacts on the Stardust collector (Westphal et al. 2008) and the clustered temporal distribution of small impacts recorded by on-board instruments (Green et al. 2007). A similar inference has been made to explain a change in optical polarization across the coma of another Jupiter family comet, 2P/Encke (Jewitt 2007). In their extensive discussion of dust fragmentation, Clark et al. (2004) suggest that most volatile ices should have sublimed well before broad dispersion into the coma, and are therefore unlikely to play a major role in aggregate strength after a few hours. However, evidence of progressive release of carbon monoxide within cometary comae (Cottin et al. 2004) perhaps reveals the presence of labile polymeric organic matter, which we suggest may have acted as a weak adhesive prior to gradual dissociation by ultra-violet irradiation, loss of vapor, creation of still further internal pore-space and unlocking of sub-grains. Some organic matter clearly survived to be collected by Stardust both in aerogel and on foils (e.g., Sandford et al. 2006; Stephan et al. 2008), and in their study of carbon and nitrogen in Wild 2 particles in aerogel, Gallien et al (2008) conclude that vaporization of surviving organic matter may even have contributed to the expansion of bulbous tracks. Kearsley et al. (2008) and Leitner et al. (2008) report carbonaceous remnants preserved around the edge of a

very complicated crater, interpreted as a rare high porosity aggregate. Matrajt et al. (2008) show that organic matter was present even within particles such as Febo. Such observations accord well with our experimental data and our interpretation of dense, but weak aggregate particle structure in Wild 2 cometary dust. Evidence from meteors generated by other Jupiter family comets (e.g., Borovička 2006; Trigo-Rodríguez and Llorca 2006) certainly suggests that their particles have low strength, although most authors have interpreted this as an indication of a delicate, primitive porous structure of low density.

Our study has shown that the internal structure of particles collected by Stardust may provide critical evidence of the mechanisms, location and timing of their formation, although much information has been lost due to capture-related processing. We are now beginning to study the state of residue preservation and the scale of compositional mixing in the smaller experimental aggregate craters (such as that in Fig. 9) by analytical TEM of crater sections cut by FIB. Despite apparently contributing only a very small fraction of the collected mass (3 to 7%, Kearsley et al. 2008), the smaller particles are especially important as we do not know if their relatively poor preservation, in both aerogel and Al foil impacts, might still conceal a population of amorphous, non-crystalline materials. Our shots of fine-grained, monodisperse, low porosity, high density aggregates onto aerogel demonstrated that they can generate bulbous Type C tracks (e.g., Fig. 9). As these aggregates contained substantial volatile-rich adhesive, whose shock-heating might aid expansion during impact, we cannot assess whether violent mechanical disaggregation is the main cause of lateral dispersion of material onto the track walls (c.f. Trigo-Rodríguez et al. 2008). We are continuing experimental investigation of the control of aerogel track morphology, using aggregates with different sub-grain sizes and compositions, and partially sintered aggregates free of adhesive. Impact of our artificial aggregates onto aerogel also raises the possibility of studying differential preservation as a function of mineral composition and grain size, as well as the entrainment of volatile organic species as molecular and isotopic tracers within the porous grains.

Acknowledgments–We thank NASA for access to the Stardust returned samples and supply of flight-spare Al foils; STFC for funding the hypervelocity impact facilities at the University of Kent; Fred Hörz, Mike Zolensky, Don Brownlee, and John Bradley for stimulating discussions about impact processes and the nature of cometary dust; and Tony Wighton for the preparation of excellent polished sections of the aggregate projectile materials. Parts of this work were performed under the auspices of the U.S. Department of Energy by Lawrence Livermore National Laboratory under Contract DE-AC52-07NA27344.

Editorial Handling—Dr. John Bradley

REFERENCES

Belton M. J. S., Thomas P., Veverka J., Schultz P., A'Hearn M. F., Feaga L., Farnham T., Groussin O., Li J.-Y., Lisse C., McFadden L., Sunshine J., Meech K. J., Delamere W. A., and Kissel J. 2007. The internal structure of Jupiter family cometary nuclei from Deep Impact observations: The "talps" or "layered pile" model. *Icarus* 187:332–344.

Bernhard R. P. and Hörz F. 1995. Craters in aluminum 1100 by sodalime glass spheres at velocities 1–7 km/s. *International Journal of Impact Engineering* 17:69–80.

Blum J., Schräpler R., Davidsson B. J. R., and Trigo-Rodríguez J. M. 2006. The physics of protoplanetesimal dust agglomerates. I. Mechanical properties and relations to primitive bodies in the solar system. *The Astrophysical Journal* 652:1768–1781.

Blum J. and Wurm G. 2000. Experiments on sticking, restructuring, and fragmentation of preplanetary dust aggregates. *Icarus* 143(1):138–46.

Blum J. and Wurm G. 2008. The growth mechanisms of macroscopic bodies in protoplanetary disks. *Annual Review of Astronomy and Astrophysics* 46:21–56.

Borovička J. 2007. Properties of meteoroids from different classes of parent bodies. In: *Near Earth objects, our celestial neighbors: Opportunity and risk*, edited by Milani A., Valsecchi G. B., and Vokrouhlický D. Proceedings, IAU Symposium No. 236. pp. 107–120.

Bradley J. P. 2004. Interplanetary dust particles. In *Meteorites, comets, and planets*, edited by Davis A. M. Treatise on Geochemistry vol. 1. Amsterdam: Elsevier. pp. 689–711.

Brownlee D., Tsou P., Aléon J., Alexander C. M. O'D., Araki T., Bajt S., Baratta G. A., Bastien R., Bland P., Bleuet P., Borg J., Bradley J. P., Brearley A., Brenker F., Brennan S., Bridges J. C., Browning N., Brucato J. R., Brucato H., Bullock E., Burchell M. J., Busemann H., Butterworth A., Chaussidon M., Cheuvront A., Chi M., Cintala M. J, Clark B. C., Clemett S. J., Cody G., Colangeli L., Cooper G., Cordier P. G., Daghlian C., Dai Z., D'Hendecourt L., Djouadi Z., Dominguez G., Duxbury T., Dworkin J. P., Ebel D., Economou T. E., Fairey S. A. J., Fallon S., Ferrini G., Ferroir T., Fleckenstein H., Floss C., Flynn G., Franchi I. A., Fries M., Gainsforth Z., Gallien J.-P., Genge M., Gilles M. K., Gillet P., Gilmour J., Glavin D. P., Gounelle M., Grady M. M., Graham G. A., Grant P. G., Green S. F., Grossemy F., Grossman L., Grossman J., Guan Y., Hagiya K., Harvey R., Heck P., Herzog G. F., Hoppe P., Hörz F., Huth J., Hutcheon I. D., Ishii H., Ito M., Jacob D., Jacobsen C., Jacobsen S., Joswiak D., Kearsley A. T., Keller L., Khodja H., Kilcoyne A. L. D., Kissel J., Krot A., Langenhorst F., Lanzirotti A., Le L., Leshin L., Leitner J., Lemelle L., Leroux H., Liu M.-C., Luening K., Lyon I., MacPherson G., Marcus M. A., Marhas K., Matrajt G., Meibom A., Mennella V., Messenger K., Mikouchi T., Mostefaoui S., Nakamura T., Nakano T., Newville M., Nittler L. R., Ohnishi I., Ohsumi K., Okudaira K., Papanastassiou D. A., Palma R., Palumbo M. O., Pepin R. E., Perkins D., Perronnet M., Pianetta P., Rao W., Rietmeijer F., Robert F., Rost D., Rotundi A., Ryan R., Sandford S. A., Schwandt C. S., See T. H., Schlutter D., Sheffield-Parker J. A., Simionovici S., Sitnitsky S. I., Snead C. J., Spencer M. K., Stadermann F. J., Steele A., Stephan T., Stroud R., Susini J., Sutton S. R., Taheri M., Taylor S., Teslich N., Tomeoka K., Tomioka N., Toppani A., Trigo-Rodríguez J. M., Troadec D., Tsuchiyama A., Tuzzolino A. J., Tyliszczak T., Uesugi K., Velbel M., Vellenga J., Vicenzi E., Vincze L., Warren J., Weber I., Weisberg M., Westphal A. J., Wirick S., Wooden D., Wopenka B., Wozniakiewicz P. J., Wright I., Yabuta H., Yano H., Young E. D., Zare R. N., Zega T., Ziegler K., Zimmerman L., Zinner E., and Zolensky M. 2006. Comet 81P/Wild 2 under a microscope. *Science* 304:1711–1716.

Brownlee D. E., Tsou P., Anderson J. D., Hanner M. S., Newburn R. L., Sekanina Z., Clark B. C., Hörz F., Zolensky M. E., Kissel J., McDonnell J. A. M., Sandford S. A., and Tuzzolino A. J. 2003. Stardust: Comet and interstellar dust sample return mission. *Journal of Geophysical Research* 108(E10), 8111, doi:10.1029/2003JE002087.

Brownlee D. E., Wheelock M. M., Temple S., Bradley J. P., and Kissel J. A. 1987. Comparison of Halley, meteorites and interplanetary dust. *Bulletin of the American Astronomical Society* 19:879.

Burchell M. J., Cole M. J., McDonnell J. A. M., and Zarnecki J. C. 1999. Hypervelocity impact studies using the 2 MV Van de Graaff dust accelerator and two stage light-gas gun of the University of Kent at Canterbury. *Measurement Science and Technology* 10: 41–50.

Burchell M. J., Fairey S. A. J., Wozniakiewicz P., Brownlee D. E., Hörz F., Kearsley A. T., See T. H., Westphal A., Green S. F., and Trigo-Rodríguez J. M. 2008. Characteristics of cometary dust tracks in Stardust aerogel and laboratory calibrations. *Meteoritics & Planetary Science* 43:23–40.

Burchell M. J., Fairey S. A. J., Foster N. J., and Cole M. J. 2009. Hypervelocity capture of particles in aerogel: Dependence on aerogel properties. *Planetary and Space Science* 57:58–70.

Burchell M. J., Graham G. A., and Kearsley A. 2006. Cosmic dust collection in aerogel. *Annual Review of Earth and Planetary Science* 34:385–418.

Burchell M. J. and Kearsley A. T. 2009. Short-period Jupiter family comets after Stardust. *Planetary and Space Science* 57:1146–1161.

Ciesla F. J. 2007. Outward transport of high-temperature materials around the midplane of the solar nebula. *Science* 318:613–615.

Clark B. C., Green S. F., Economou T. E., Sandford S. A., Zolensky M. E., McBride N., and Brownlee D. E. 2004. Release and fragmentation of aggregates to produce heterogeneous, lumpy coma streams. *Journal of Geophysical Research* 109, E12S03, 1–13, doi:10.1029/2004JE002319.

Consolmagno G. J., Britt D., and Macke R. J. 2008. The significance of meteorite density and porosity. *Chemie der Erde (Geochemistry)* 68:1–29.

Corrigan C., Zolensky M. E., Dahl J., Long M., Weir J., Sapp C., and Burkett P. J. 1997. The porosity and permeability of chondritic meteorites and interplanetary dust particles. *Meteoritics & Planetary Science* 32:509–515.

Cottin H., Bénilan Y., Gazeau M.-C., and Raulin F. 2004. Origin of cometary extended sources from degradation of refractory organics on grains: Polyoxymethylene as formaldehyde parent molecule. *Icarus* 167:397–416.

Cour-Palais B. G. 1987. Hypervelocity impact in metals, glass, and composites. *International Journal of Impact Engineering* 5: 221–237.

Davidsson B. J. R. and Gutiérrez P. J. 2006. Non-gravitational force modeling of comet 81P/Wild 2. I. A nucleus bulk density estimate. *Icarus* 180:224–242.

Dello Russo N., Weaver H. A., Lisse C. M., and Vervack R. J. 2006. Comet chemistry: Obtaining clues to the formation and evolution of the solar system with high-resolution infrared spectroscopy. *John Hopkins APL Technical Digest* 27:121–132.

Dominguez G., Westphal A. J., Jones S. M., and Phillips M. L. F. 2004. Energy loss and impact cratering in aerogels: theory and experiment. *Icarus* 172:613–624.

Dominik C., Blum J., Cuzzi J. N., and Wurm G. 2007. Growth of dust as the initial step toward planet formation. In *Protostars and planets*, edited by Reipurth B., Jewitt D., and Keil K. Tucson, Arizona: The University of Arizona Press. pp. 783–800.

Donn B. 1990. The formation and structure of fluffy cometary nuclei from random accumulation of grains. *Astronomy and Astrophysics* 235:441–446.

Donn B. 1991. The accumulation and structure of comets. In *Comets in the post-Halley era*, vol. 1, edited by Newburn R. L. Jr., Neugebauer M., and Rahe J. Dordrecht: Kluwer Academic Publishers. pp. 335–359.

Eichhorn K. and Grün E. 1993. High-velocity impacts of dust particles in low temperature water ice. *Planetary and Space Science* 41:429–433.

Flynn G. J. 2008. Physical, chemical, and mineralogical properties of comet 81P/Wild 2 particles collected by Stardust. *Earth, Moon, and Planets* 102:447–459.

Flynn G., Bleuet P., Borg J., Bradley J. P., Brenker F., Brennan S., Bridges J. C. Brownlee D. E., Bullock E., Burghammer M., Clark B. C., Dai Z. R., Daghlian C. P., Djouadi Z., Fakra S., Ferroir T., Floss C., Franchi I. A., Gainsforth Z., Gallien J.-P., Gillet P., Grant P. G., Graham G. A., Grossemy F., Heck P., Herzog G. F., Hoppe P., Hörz F., Huth J., Ignatyev K., Ishii H., Janssens K., Joswiak D., Kearsley A. T., Khodja H., Lanzirotti A., Leitner J., Lemelle L., Leroux H., Luening K., MacPherson G., Marhas K., Matrajt G., Nakamura T., Nakamura-Messenger K., Nakano T., Newville M., Papanastassiou D. A., Pianetta P., Rao W., Riekel C., Rietmeijer F., Rost D., Schwandt C. S., See T. H., Sheffield-Parker J. A., Simionovici S., Sitnitsky S. I., Snead C. J., Stadermann F. J., Stephan T., Stroud R. M., Susini J.,. Suzuki Y., Sutton S. R., Taylor S., Teslich N., Troadec D., Tsou P., Tsuchiyama A., Uesugi K., Vekemans B., Vicenzi E., Vincze L., Westphal A. J., Wozniakiewicz P. J., Zinner E., and Zolensky M. 2006. Elemental composition of comet 81P/Wild 2 samples collected by Stardust. *Science* 314:1731–1735.

Foster N. J., Kearsley A. T., Burchell M. J., Wozniakiewicz P. J., Creighton J. A., and Cole M. J. 2008. Analysis of Hydrous Phyllosilicates in Stardust type B tracks (abstract #8209). 2008 Asteroids, Meteors and Comets Conference.

Fulle M., Levasseur-Regourd A. C., McBride N., and Hadamcik N. 2000. In-situ dust measurements from within the coma of 1P/Halley: First order approximation with a dynamical dust model. *Astronomical Journal* 119:1968–1977.

Gallien J.-P., Khodja H., Herzog G. F., Taylor S., Koepsell E., Daghlian C. P., Flynn G. J., Sitnitsky I., Lanzirotti A., Sutton S. R., and Keller L. P 2008. Characterization of carbon- and nitrogen-rich particle fragments captured from comet 81P/Wild 2. *Meteoritics & Planetary Science* 43:335–351.

Graham G. A., Kearsley A. T., Wright I. P., Grady M. M., Drolshagen G., McBride N. M., Green S. F., Burchell M. J., Yano H., and Elliott R. 2001. Analysis of impact residues on spacecraft surfaces: possibilities and problems. In *Proceedings of the 3rd European Conference on Space Debris*, edited by Sawaya-Lacoste, H. ESA Special Publication 473. European Space Agency, Noordwijk. pp. 197–203.

Graham G. A., Bradley J. P., Dai Z. R., Kearsley A. T., Bernas M., and Snead C. 2005. Great expectations—Dust recovered from aerogel (abstract #4089). In *Dust in planetary systems.* LPI Contribution #1280. pp. 56–57.

Graham G. A., Kearsley A. T., Wright I. P., Burchell M. J., and Taylor E. A. 2003. Observations on hypervelocity impact damage sustained by multi-layered insulation foils exposed in low Earth orbit and simulated in the laboratory. *International Journal of Impact Engineering* 29:307–316.

Green S. F., McBride N., Colwell M. T. S. H., McDonnell J. A. M., Tuzzolino A. J., Economou T. E., Clark B. C., Sekanina Z., Tsou P., and Brownlee D. E. 2007. Stardust Wild 2 dust measurements. In *Dust in planetary systems*, edited by Krueger H. and Graps A. ESA SP-643. pp. 35–44.

Greenberg J. M. 1987. Comet Halley: A carrier of interstellar dust chemical evolution. *Advances in Space Research* 7.5:33–44.

Greenberg J. M., Zhao N. S., and Hage J. I. 1989. The interstellar dust

model of comet dust constrained by 3.4 μm and 10 μm emission. *Advances in Space Research* 9:3–11.

Hanner M. S. 1984. A comparison of dust properties in recent periodic comets. *Advances in Space Research* 4:189–196.

Hörz F., Cintala M. J., See T. H., and Nakamura-Messenger K. 2009. Penetration tracks in aerogel produced by Al_2O_3 spheres. *Meteoritics & Planetary Science* 44:1243–1264.

Hörz F., Cintala M. J., Zolensky M. E., Bernhard R. B., Davidson W. E., Haynes G., See T. H., Tsou P., and Brownlee D. E. 1998. Capture of hypervelocity particles with low density aerogel. NASA TM-98–201792. 58 p.

Hörz F., Bastien R., Borg J., Bradley J. P., Bridges J. C., Brownlee D. E., Burchell M. J., Cintala M. J., Dai Z. R., Djouadi Z., Dominguez G., Economou T. E., Fairey S. A. J., Floss C., Franchi I. A., Graham G. A., Green S. F., Heck H., Hoppe P., Huth J., Ishii H., Kearsley A. T., Kissel J., Leitner J., Leroux H., Marhas M., Messenger K., Schwandt C. S., See T. H., Snead S., Stadermann F. J., Stephan T., Stroud R., Teslich N., Trigo-Rodríguez J. M., Tuzzolino A. J., Troadec D., Tsou P., Warren J., Westphal A., Wozniakiewicz P. J., Wright I., and Zinner E. 2006. Impact features on Stardust: Implications for comet 81P/Wild 2 dust. *Science* 314:1716–1719.

Iatì M. A., Saija R., Giusto A., Dentia P., Borghese F., and Cecchi-Pestellini C. 2004. Optical properties of interstellar grain aggregates. *Journal of Quantitative Spectroscopy & Radiative Transfer* 89:43–51.

Ishii H., Bradley J. P., Dai Z. R., Chi M., Kearsley A. T., Burchell M. J., Browning N. D., and Molster F. J. 2008. Comparison of 81P/Wild 2 dust with interplanetary dust from comets. *Science* 319:447–450.

Jewitt D. 2007. Looking through the HIPPO: Nucleus and dust in comet 2P/Encke. *The Astronomical Journal* 128:3061–3069.

Jewitt D. and Matthews H. 1999. Particulate mass loss from comet Hale-Bopp. *The Astrophysical Journal* 117:1056–1062.

Jewitt D. and Meech K. J. 1986. Cometary grain scattering versus wavelength, or, "What color is comet dust." *The Astrophysical Journal* 310:937–952.

Kearsley A. T., Borg J., Graham G. A., Burchell M. J., Cole M. J., Leroux H., Bridges J. C., Hörz F., Wozniakiewicz P. J., Bland P. A., Bradley J. P., Dai Z. R., Teslich N., See T., Hoppe P., Heck P. R., Huth J., Stadermann F. J., Floss C., Marhas K., Stephan T., and Leitner J. 2008a. Dust from comet Wild 2: Interpreting particle size, shape, structure and composition from impact features on the Stardust aluminum foils. *Meteoritics & Planetary Science* 43: 41–74.

Kearsley A. T., Burchell M. J., Hörz F., Cole M. J., and Schwandt C. S. 2006. Laboratory simulation of impacts upon aluminum foils of the Stardust spacecraft: Calibration of dust particle size from comet Wild 2. *Meteoritics & Planetary Science* 43:167–180.

Kearsley A. T., Graham G. A., Burchell M. J., Cole M. J., Dai Z., Teslich N., Chater R. J., Wozniakiewicz P., Spratt J., and Jones G. 2007. Analytical scanning and transmission electron microscopy of laboratory impacts on Stardust aluminum foils: Interpreting impact crater morphology and the composition of impact residues. *Meteoritics & Planetary Science* 42:191–210.

Kearsley A. T., Graham G. A., Burchell M. J., Cole M. J., Wozniakiewicz P., Teslich N., Bringa E., Hörz F., Blum J., and Poppe T. 2008b. Micro-craters in aluminum foils on NASA's Stardust spacecraft: Implications for dust particles emanating from comet Wild 2. *International Journal of Impact Engineering* 35:1616–1624.

Lanzirotti A., Sutton S. R., Flynn G. J., Newville A., and Rao W. 2008. Chemical composition and heterogeneity of Wild 2 cometary particles determined by synchrotron X-ray fluorescence. *Meteoritics & Planetary Science* 43:187–213.

Leitner J., Stephan T., Kearsley A. T., Hörz F., Flynn G. J., and Sandford S. A. 2008. TOF-SIMS analysis of crater residues from Wild 2 cometary particles on Stardust aluminum foil. *Meteoritics & Planetary Science* 43:161–186.

Leroux H., Rietmeijer F. J. M., Velbel M. A., Brearley A. J., Jacob D., Langenhorst F., Bridges J. C., Zega T. J., Stroud R. M., Cordier P., Harvey R. P., Lee M., Gounelle M., and Zolensky M. E. 2008a. A TEM study of thermally modified comet 81P/Wild 2 dust particles by interactions with the aerogel matrix during the Stardust capture process. *Meteoritics & Planetary Science* 43:97–120.

Leroux H., Stroud R. M., Dai Z. R., Graham G. A., Troadec D., Bradley J. P., Teslich N., Borg J., Kearsley A. T., and Hörz F. 2008b. Transmission electron microscopy of cometary residues from micron-sized craters in the Stardust Al foils. *Meteoritics & Planetary Science* 43:143–160.

Levasseur-Regourd A. C., Hadamcik E., Desvoivres E., and Lasue J. 2009. Probing the internal structure of the nuclei of comets. *Planetary and Space Science* 57:221–228.

Levasseur-Regourd A. C., Zolensky M., and Lasue J. 2008. Dust in cometary comae: Present understanding of the structure and composition of dust particles. *Planetary and Space Science* 56: 1719–1724.

McKeegan K. D., Aléon, J., Bradley J., Brownlee D., Busemann H., Butterworth A., Chaussidon M., Fallon S., Floss C., Gilmour J., Gounelle M., Graham G., Guan Y., Heck P. R., Hoppe P., Hutcheon I. D., Huth J., Ishii H., Ito M., Jacobsen S. B., Kearsley A., Leshin L. A., Liu M.-C., Lyon I., Marhas K., Marty B., Matrajt G., Meibom A., Messenger S., Mostefaoui S., Mukhopadhyay S., Nakamura-Messenger K., Nittler L., Palma R., Pepin R. O., Papanastassiou D. A., Robert F., Schlutter D., Snead C. J., Stadermann F. J., Stroud R., Tsou P., Westphal A., Young E. D., Ziegler K., Zimmermann L., and Zinner E. 2006. Isotopic compositions of cometary matter returned by Stardust. *Science* 314:1724–1728.

Nakamura R. 1998. Optical properties of dust aggregates in the disk of Beta Pictoris. *Earth Planets Space* 50:587–593.

Nakamura T., Tsuchiyama A., Akaki T., Uesugi K., Nakano T., Takeuchi A., Suzuki Y., and Noguchi T. 2008. Bulk mineralogy and three-dimensional structures of individual Stardust particles deduced from synchrotron X-ray diffraction and microtomography analysis. *Meteoritics & Planetary Science* 43: 247–259.

Nguyen A. N., Busemann, H., and Nittler L. R. 2007. Remarkably high abundance of presolar grains in interplanetary dust particles collected from the comet Grigg-Skjellerup dust stream (abstract #2332). 38th Lunar and Planetary Science Conference. CD-ROM.

Noguchi T., Nakamura T., Okudaira K., Yano H., Sugita S., and Burchell, M. J. 2007. Thermal alteration of hydrated minerals during hypervelocity capture to silica aerogel at the flyby speed of STARDUST. *Meteoritics & Planetary Science* 42:357–372.

Ohsumi K., Hagiya K., Mikouchi T., and Zolensky M. E. 2008. Synchrotron X-ray diffraction studies of olivine from comet Wild 2 (abstract #1808). 39th Lunar and Planetary Science Conference. CD-ROM.

Ormel C. W., Spaans M., and Tielens A. G. G. M. 2007 Dust coagulation in protoplanetary disks: Porosity matters. *Astronomy & Astrophysics* 461:215–232.

Price M. C., Kearsley A. T. Burchell M. J., Hörz F., and Cole M. J. 2009. Comet 81P/Wild 2: The updated Stardust coma dust fluence measurement for smaller (sub 10-micrometer) particles (abstract #1564). 40th Lunar and Planetary Science Conference. CD-ROM.

Rietmeijer F. J. M. and Mackinnon I. D. R. 1987. Cometary evolution: Clues to physical properties from chondritic interplanetary dust particles. In *The diversity and similarity of*

comets, edited by Rolfe E. J. and Battrick B. ESA Special Publication #278. Noordwijk: European Space Agency. pp. 363–367.

Rudolph V. 1968. Untersuchungen an Kratern von Mikroprojektilen im Geschwindigkeitsbereich von 0.5 bis 10 km/s. *Zeitschrift für Naturforschung* 24a:326–331.

Sandford S. A., Aléon J., Alexander C. M. O. D., Araki T., Bajt S., Baratta G. A., Borg J., Bradley J. P., Brownlee D. E., Brucato J. R., Burchell M. J., Busemann H., Butterworth A., Clemett S. J., Cody G., Colangeli L., Cooper G., D'Hendecourt L., Djouadi Z., Dworkin J. P., Ferrini G., Fleckenstein H., Flynn G. J., Franchi I. A., Fries M., Gilles M. K., Glavin D. P., Gounelle M., Grossemy F., Jacobsen C., Keller L. P., Kilcoyne A. L. D., Leitner J., Matrajt G., Meibom A., Mennella V., Mostefaoui S., Nittler L. R., Palumbo M. E., Papanastassiou D. A., Robert F., Rotundi A., Snead C. J., Spencer M. K., Stadermann F. J., Steele A., Stephan T., Tsou P., Tyliszczak T., Westphal A. J., Wirick S., Wopenka B., Yabuta H., Zare R. N., and Zolensky M. E. 2006. Organics captured from comet 81P/Wild 2 by the Stardust spacecraft. *Science* 314:1720–1724.

Stadermann F. J., Hoppe H., Floss C., Heck P. R., Hörz F., Huth J., Kearsley A. T., Leitner J., Marhas K. K., McKeegan K. D., and Stephan T. 2008 Stardust in Stardust—The C, N, and O isotopic compositions of Wild 2 cometary matter in Al foil impacts. *Meteoritics & Planetary Science* 43:299–313.

Stadermann F. J., Floss C., and Bose M. 2007. Correlated high spatial resolution elemental and isotopic characterisation of Wild 2 cometary samples (abstract #1334). 38th Lunar and Planetary Science Conference. CD-ROM.

Stephan T., Rost D., Vicenzi E. P., Bullock E. S., MacPherson G. J., Westphal A. J., Snead C. J., Flynn G. J., Sandford S., and Zolensky M. E. 2008. TOF-SIMS analysis of cometary matter in Stardust aerogel tracks. *Meteoritics & Planetary Science* 43:233–246.

Tomeoka K., Tomioka N., and Ohnishi I. 2008. Silicate minerals and Si-O glass in comet Wild 2 samples: Transmission electron microscopy. *Meteoritics & Planetary Science* 43:273–284.

Trigo-Rodríguez J. M. and Blum J. 2009. Tensile strength as an indicator of the degree of primitiveness of undifferentiated bodies. *Planetary and Space Science* 57:243–249.

Trigo-Rodríguez J. M. and Llorca J. 2006. The strength of cometary meteoroids: Clues to the structure and evolution of comets. *Monthly Notices of the Royal Astronomical Society* 372:655–660.

Trigo-Rodríguez J. M., Dominguez G., Burchell M. J., Hörz F., and Llorca J. 2008. Bulbous tracks arising from hypervelocity capture in aerogel. *Meteoritics & Planetary Science* 43:75–86.

Tsou P., Brownlee D. E., Anderson J. D., Bhaskaran S., Cheuvront A. R., Clark B. C., Duxbury T., Economou T., Green S. F., Hanner M. S., Hörz F., Kissel J., McDonnell J. A. M., Newburn R. L., Ryan R. E., Sandford S. A., Sekanina Z., Tuzzolino A. J., Vellinga J. M., and Zolensky M. E. 2004. Stardust encounters comet 81P/Wild 2. *Journal of Geophysical Research* E 109(E12), E12S01, 1–8, doi:10.1029/2004JE002317.

Tuzzolino A. J., Economou T. E., Clark B. C., Tsou P., Brownlee D. E., Green S. F., McDonnell J. A. M., McBride N., and Colwell M. T. S. H. 2004. Dust measurements in the coma of comet 81P/Wild 2 by the dust flux monitor instrument. *Science* 304:1776–1780.

Velbel M. and Harvey R. P. 2007. Sulfide–metal textural relations in an extensively melted Stardust grain from comet 81P/Wild 2. *Meteoritics & Planetary Science* 42:A155.

Wasson J. 1995. Chondrites: The compaction of fine matrix and matrixlike chondrule rims. *Meteoritics* 30:594.

Weidling R., Güttler C., Blum J., and Brauer F. 2009. The physics of protoplanetesimal dust agglomerates. III. compaction in multiple collisions. *The Astrophysical Journal* 696:2036–2048.

Weissman P. R., Asphaug E., and Lowry S. C. 2005. Structure and density of cometary nuclei. In *Comets II,* edited by Festou M. C., Keller H. U., and Weaver H. A. Tucson: The University of Arizona Press. pp. 337–357.

Westphal A. J., Bastien R. K., Borg J., Bridges J., Brownlee D. E., Burchell M. J., Cheng A. F., Clark B. C., Djouadi Z., Floss C., Franchi I., Gainsforth Z., Graham G., Green S. F., Heck P. R., Horányi M., Hoppe P., Hörz F. P., Huth J., Kearsley A., Leroux H., Marhas K., Nakamura-Messenger K., Sandford S. A., See T. H., Stadermann F. J., Teslich N. E., Tsitrin S., Warren J. L., Wozniakiewicz P. J., and Zolensky M. E. 2008. Discovery of non-random spatial distribution of impacts in the Stardust cometary collector. *Meteoritics & Planetary Science* 43:415–429.

Wozniakiewicz P. J., Kearsley A. T., Burchell M. J., Bland P. A., Ishii H. A., Dai Z. R., Teslich N., Collins G., Bradley J. P., Russell S., Cole M. J., and Lee M. 2008. Constraining the effects of capture-heating on chemistry and structure of cometary sulphides under Stardust encounter conditions (abstract #1791). 39th Lunar and Planetary Science Conference. CD-ROM.

Zhukovska S., Gail H.-P., and Trieloff M. 2008. Evolution of interstellar dust and stardust in the solar neighbourhood. *Astronomy and Astrophysics* 479:453–480.

Zolensky M. E., Zega T. J., Yano H., Wirick S., Westphal A. J., Weisberg M. K., Weber I., Warren J. L., Velbel M. A., Tsuchiyama A., Tsou P, Toppani A., Tomioka N, Tomeoka K., Teslich N., Taheri M., Susini J., Stroud R., Stephan T., Stadermann F. J., Snead C. J., Simon S. B., Simionovici A., See T. H., Robert F., Rietmeijer F. J. M., Rao W., Perronnet M. C., Papanastassiou D. A., Okudaira K., Ohsumi K., Ohnishi I., Nakamura-Messenger K., Nakamura T., Mostefaoui S., Mikouchi T., Meibom A., Matrajt G., Marcus M. A., Leroux H., Lemelle L., Le L., Lanzirotti A., Langenhorst F., Krot A. N., Keller L. P., Kearsley A. T., Joswiak D., Jacob D., Ishii H., Harvey R., Hagiya K., Grossman L., Grossman, J. N., Graham G. A., Gounelle M., Gillet P., Genge M. J., Flynn G., Ferroir T., Fallon S., Ebel D. S., Dai Z. R., Cordier P., Clark B., Chi M., Butterworth A. L., Brownlee D. E., Bridges J. C., Brennan S., Brearley A., Bradley J. P., Bleuet P., Bland P. A., and Bastien R. 2006. Mineralogy and petrology of comet Wild 2 nucleus samples. *Science* 314:1735–1739.

Zolensky M., Nakamura-Messenger K., Rietmeijer F., Leroux H., Mikouchi T., Ohsumi K., Simon S., Grossman L., Stephan T., Weisberg M., Velbel M., Zega T., Stroud R., Tomeoka K., Ohnishi I., Tomioka N., Nakamura T., Matrajt G., Joswiak D., Brownlee D., Langenhorst F., Krot A., Kearsley A., Ishii H., Graham G., Dai Z. R., Chi M., Bradley J., Hagiya K., Gounelle M., Keller L., and Bridges J. 2008. Comparing Wild 2 particles to chondrites and IDPs. *Meteoritics & Planetary Science* 43:261–272.